(2)

WL-TR-92-3012

THE 12-METER TRUSS ACTIVE CONTROL EXPERIMENT DESIGN, ANALYSIS & OPEN-LOOP TESTING

ROBERT W. GORDON
Structural Dynamics Branch
Structures Division

Final Report for Period JUN 88 - DEC 90

April 1992

Approved for Public Release;
Distribution is Unlimited

FLIGHT DYNAMICS DIRECTORATE
WRIGHT LABORATORY
AIR FORCE SYSTEMS COMMAND
WRIGHT-PATTERSON AFB, OH 45433-6553

NOTICE

When Government drawings, specifications, or other data are used for any purpose other than in connection with a definitely Government-related procurement, the United States Government incurs no responsibility or any obligation whatsoever. The fact that the Government may have formulated or in any way supplied the said drawings, specifications, or other data, is not to be regarded by implication, or otherwise in any manner construed, as licensing the holder, or any other person or corporation; or as conveying any rights or permission to manufacture, use, or sell any patented invention that may in any way be related thereto.

This report is releasable to the National Technical Information Service (NTIS). At NTIS, it will be available to the general public, including foreign nationals.

This technical report has been reviewed and is approved for publication.

Robert W. Gordon

ROBERT W GORDON
Aerospace Engineer

Stephen R Whitehouse

STEPHEN R WHITEHOUSE, Maj, USAF
Technical Manager, Vibration Group

FOR THE COMMANDER

Jerome Pearson

JEROME PEARSON
Chief, Structural Dynamics Branch

If your address has changed, if you wish to be removed from our mailing list, or if the addressee is no longer employed by your organization please notify WL/FIBGC, WPAFB, OH 45433-6553 to help us maintain a current mailing list.

Copies of this report should not be returned unless return is required by security considerations, contractual obligations, or notice on a specified document.

REPORT DOCUMENTATION PAGE

Form Approved
OMB No. 0704-0188

1. AGENCY USE ONLY *(Leave blank)*	2. REPORT DATE	3. REPORT TYPE AND DATES COVERED
	APRIL 1992	FINAL JUN 88 - DEC 90

4. TITLE AND SUBTITLE
THE 12-METER TRUSS ACTIVE CONTROL EXPERIMENT; DESIGN, ANALYSIS AND OPEN-LOOP TESTING

5. FUNDING NUMBERS
PE 62201F
PR 2401
TA 04
WU 24010432

6. AUTHOR(S)
ROBERT W. GORDON (513) 255-5236 EXT 402

7. PERFORMING ORGANIZATION NAME(S) AND ADDRESS(ES)
STRUCTURAL DYNAMICS BRANCH
STRUCTURES DIVISION
FLIGHT DYNAMICS DIRECTORATE
WRIGHT LABORATORY
WRIGHT-PATTERSON AFB OH 45433-6553

8. PERFORMING ORGANIZATION REPORT NUMBER
WL-TR-92-3012

9. SPONSORING/MONITORING AGENCY NAME(S) AND ADDRESS(ES)

10. SPONSORING/MONITORING AGENCY REPORT NUMBER

11. SUPPLEMENTARY NOTES

12a. DISTRIBUTION/AVAILABILITY STATEMENT
APPROVED FOR PUBLIC RELEASE; DISTRIBTION IS UNLIMITED

12b. DISTRIBUTION CODE

13. ABSTRACT *(Maximum 200 words)*

This report documents the design, analysis and open-loop testing of the 12-Meter Truss Active Control Experiment at Wright Laboratory. The objectives of the experiment were to develop a test bed which was respresentative of the dynamic characteristics of future large space systems and then evaluate the performance of leading active vibration control approaches applied to the test bed. The experimental hardware consisted of a 12-meter-long aluminum truss beam equipped with eight linear momentum exchange actuators and colocated accelerometer sensors and a fast digital control computer. The report describes in detail experiment design and hardware development activities, open-loop analysis and performance prediction, and open-loop experimental testing of the final experiment.

14. SUBJECT TERMS	15. NUMBER OF PAGES
ACTIVE VIBRATION CONTROL SPACE STRUCTURES ACTUATORS	64
	16. PRICE CODE

17. SECURITY CLASSIFICATION OF REPORT	18. SECURITY CLASSIFICATION OF THIS PAGE	19. SECURITY CLASSIFICATION OF ABSTRACT	20. LIMITATION OF ABSTRACT
UNCLASSIFIED	UNCLASSIFIED	UNCLASSIFIED	SAR

FOREWORD

This report describes work performed at Wright Laboratory, Flight Dynamics Directorate, Structures Division, Structural Dynamics Branch from August 1990 to February 1991. The work was directed by Robert W. Gordon (WL/FIBGC) as Project Engineer under Project 2401, "Structural Mechanics," Task 04, "Vibration Prediction and Control, Measurement and Analysis," Work Unit 24010432, Large Space Structures Technology Program.

TABLE OF CONTENTS

LIST OF FIGURES

LIST OF TABLES

1.0 INTRODUCTION

Many future Air Force space systems will have very challenging requirements for line-of-sight pointing, shape control or other performance metrics. These systems will also be larger and more flexible than their predecessors due to mission and minimum launch weight requirements. As a result, these systems will have an unprecedented need for vibration control to meet performance requirements. To meet this need, the Flight Dynamics Directorate of the Wright Laboratory is conducting an in-house experimental research program in the dynamics and control of flexible space structures. The 12-Meter Truss Active Vibration Control Experiment is a part of this in-house program and addresses the evaluation of state-of-the-art active vibration control approaches in realistic hardware.

1.1 Scope -- This report documents the design, analysis and open-loop testing conducted in support of the 12-Meter Truss Active Control Experiment, as part of the Large Space Structures Technology Program. Closed-loop active control design and testing haves been documented in a separate report [1].

1.2 Objectives -- The primary objective of the experiment was to evaluate the performance of state-of-the-art active vibration control approaches on a structure possessing the dynamic response and control hardware characteristics representative of future space systems. A second objective was to evaluate the performance of a new real-time digital control computer for simultaneous closed-loop vibration control, data acquisition and overall experiment control.

1.3 Background -- Since the late 1970's, a large body of theoretical research has been directed toward active vibration control approaches for flexible space structures. Much of this work has neglected real hardware effects such as sensor and actuator dynamics and finite sample times to simplify the analysis. The Large Space Structures Technology Program (LSSTP) was initiated in 1985 in the Flight Dynamics Directorate to experimentally investigate space structure dynamics and control and thus address many of the physical implementation issues neglected in previous theoretical studies. The approach of the LSSTP was to conduct a series of experiments on representative structures which focused on three major technology areas: ground test and zero-gravity

simulation, passive and active vibration control and active control hardware.

The 12-Meter Truss Active Control Experiment described in this report was the third in a series of active vibration control experiments conducted under the LSSTP. The first experiment was begun in 1985 as a simple introduction to active vibration control. The testbed consisted of an aluminum cantilever beam with an electromagnetic shaker as an actuator and a linear variable differential transformer (LVDT) as a sensor. The control objective was to add damping to the bending modes of the beam. The second experiment was designed to address two important features of future large space structures, namely, non-grounded sensors and actuators and multiple, closely spaced modes, which were not included in the first experiment. The Advanced Beam Experiment was composed of a slender aluminum beam, oriented vertically and fixed at the top end, with four momentum exchange actuators and collocated accelerometers mounted at the free end. The beam was designed so that the fundamental modes in the two bending directions and the first torsion mode were close in frequency. Some success was achieved in adding damping via active control to the three lowest modes of the beam, but, more importantly, much was learned about the behavior of flexible structures with momentum exchange actuators for vibration control. The experience gained from the Advanced Beam Experiment would prove valuable in the design of the large flexible structures experiment that would follow, namely the 12-Meter Truss Active Control Experiment. A summary of the Advanced Beam Experiment can be found in [1].

In addition to active vibration control, considerable effort was focused on ground test methods and modal parameter identification of large flexible structures. Two 12-meter-long truss beams were fabricated as test articles for this investigation; one with light damping and one with significant added damping. Modal surveys were conducted on these trusses in two configurations: vertical cantilevered from the floor and horizontally mounted on a low restraint suspension system. The lightly damped 12-meter truss was selected as the test article for the third active vibration control experiment since it had been very well characterized and was available. The design process for the experiment is discussed in detail in the next section.

2.0 EXPERIMENT DESIGN

Future large flexible space structures will have several important dynamic characteristics in common. In designing the 12-Meter Truss Active Control Experiment it was important that these characteristics be included. This section discusses the design process for the experiment including how the salient dynamic characteristics were included as design goals, the selection of the 12-meter truss configuration, selection and location of sensors and actuators, and the determination of a measurable figure-of-merit for dynamic performance.

2.1 Design Goals -- The primary design goal was to ensure that the experiment embodied the structural dynamic characteristics which will be common to many future large flexible space structures. These characteristics include natural frequencies at or below 1 Hz, high modal density at low frequencies, modal damping ratios of less than 1% of critical in global, low frequency modes and truss-type structures. Second, it was important to use nongrounded active control sensors and actuators since grounded devices could not be used on a real space structure. In addition, it was important for the experiment to have a directly measurable figure-of-merit indicative of system performance. All future systems will have at least one performance requirement, such as line-of-sight pointing error or root mean square (rms) shape error, which drives the structural dynamics and control system design. This figure-of-merit would be used as the control design objective and to directly measure experimental closed-loop performance. Finally, it was desirable to have an unconstrained structure to at least partially simulate the zero gravity environment of space.

2.2 Selection of the 12-Meter Truss -- Reaching a design which satisfied the goals described above was constrained by the practical reality of budget limitations within the LSSTP. This constraint limited the design to the use of off-the-shelf hardware as much as possible, especially for the sensors, actuators and associated electronics. After all, the objective of the experiment was to evaluate active control performance, not to develop new control hardware. Therefore, it was logical to take advantage of the 12-meter trusses, a pair of test bed structures which had been used extensively at FIBG for modal testing and ground test methods development. The existing finite element models and modal data for the trusses would mean a savings in the analysis and test time required to develop the experiment.

Table 1. Measured Frequencies and Damping of the Undamped 12-Meter Truss

Mode	Vertical Cantilever		Horizontal Free-Free	
	Frequency (Hz)	Damping (%)	Frequency (Hz)	Damping (%)
1st X Bending	2.26	0.2	12.38	0.7
1st Y Bending	2.25	0.2	12.65	0.1
1st Torsion	7.10	0.3	14.10	0.3
2nd X Bending	10.72	0.2	25.61	0.2
2nd Y Bending	10.72	0.2	25.34	0.2
2nd Torsion	21.27	0.3	27.83	0.2

The 12-meter trusses are slender truss beams with welded tubular aluminum alloy frames and a 20 inch square cross section. Each truss has 4 bolt-together sections with 4 truss bays per section for a total of 16 bays. One of the trusses is designed to have low modal damping in the low frequency bending and torsion modes. This is achieved by using low loss Lexan tubing for the bolt-in diagonal members. The other truss is designed to have significant damping in the low frequency modes by incorporating a viscoelastic axial damper in the diagonal members. The trusses are shown in a vertical cantilever test configuration in Figure 1.

The lightly damped truss in a vertical cantilever configuration met the primary design goals for the experiment of multiple, low frequency modes and light damping. Table 1 lists the frequencies and modal damping ratios for the lightly damped truss in both cantilever and unconstrained configurations. The cantilever truss has a pair of first bending modes at approximately 2.2 Hz and five global modes below 11 Hz. The truss has modal damping ratios in the range of 0.2% - 0.3% for these modes. The cantilevered truss, however, does not meet the goal of an unconstrained structure. The frequencies for the lightly damped truss suspended horizontally on a soft suspension system are considerably higher than the cantilever configuration, with the lowest frequency above 12 Hz. These frequencies were above the desired range for LSS. The addition of mass to lower the frequencies was considered, but the amount required to lower the

Figure 1. 12 Meter Trusses in the Cantilever Test Configuration

fundamental mode to the 1-2 Hz frequency range was too large for the suspension system. Thus, the lightly damped truss in the vertical cantilever configuration was chosen as the test structure for the experiment.

2.3 Sensor and Actuator Selection and Location -- The selection of sensors and actuators for the 12-Meter Truss Active Control Experiment was driven by the need to minimize development cost and time. The purpose of the experiment was to evaluate active control approaches, not develop control hardware. Much advantage was taken from the control hardware development performed on the Passive and Active Control of Space Structures (PACOSS) contract performed by Martin Marietta Astronautics Group in Denver, Colorado [3]. Experience on the Advanced Beam Experiment [2] at Wright Laboratory and the Vibration Control of Space Structures (VCOSS II) [4] contract with TRW Space and Technology Group also influenced the selection. Linear momentum exchange actuators were selected for use on the experiment due to their proven performance on these and other projects. Other candidate actuators included angular momentum exchange actuators and air jet thrusters, but lack of experience with these devices made them less desirable. The PACOSS actuator shown in Figure 2 was chosen as the baseline actuator design. It is capable of 1 pound peak force output in a frequency range from below 1 Hz to well above the 50 Hz analysis limit for the experiment. Linear structural velocity was the measurement desired for active feedback with the linear force actuators and could be implemented easily by either analog or digital integration of an accelerometer signal. Collocation of the actuators and sensors was chosen as the baseline control configuration with the option for noncollocated sensors to be used at a later date, if desired. More detailed information on the sensors and actuators used in the experiment, and their characterization, is presented in Section 3.

2.4 Sensor and Actuator Location -- Locations for the collocated sensors and actuators were selected using a few simple guidelines. First, actuators could only be located at the major truss section joints, i.e., at the 1/4, 1/2, 3/4 and tip stations. This was because mounting plates for the actuators could be attached to the truss most easily at these locations. Second, the lowest three bending mode pairs and the lowest two torsion modes would be actively controlled. In a real system design, the modes to be controlled would be dictated by their participation in one or more performance figures-of-merit. However, in this experiment, the actuator locations were selected well before a performance figure-of-merit was considered. The lowest eight truss modes were selected to provide several modes, both bending and torsion, in a frequency band of a least one

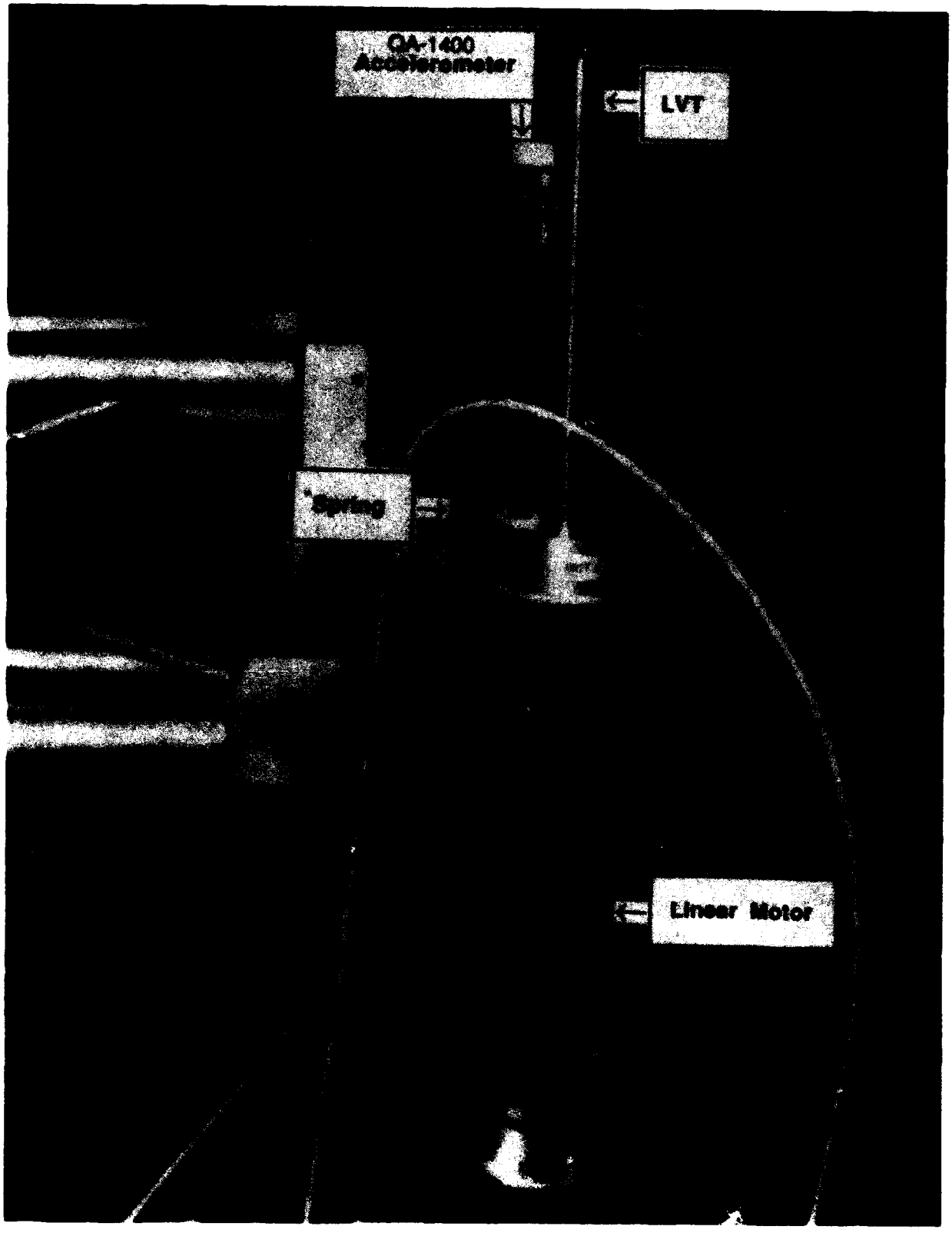

Figure 2. PACOSS Linear Momentum Exchange Actuator

decade. Third, up to eight actuators could be used. Again, this was an arbitrary decision, but it allowed the use of multiple actuators at several truss locations. Finally, actuators would be located so as to produce uncoupled bending and torsion inputs. This necessitated the use of symmetric pairs of actuators commanded out-of-phase to control torsion modes and in-phase for bending modes.

The sensor and actuator locations for the experiment were selected using the guidelines discussed above and are shown in Figure 3. Two symmetric pairs of actuators were located at the truss tip to provide both bending and torsion control. This location provided the best observability/controllability for all the modes to be controlled except the third bending mode pair. In addition, single actuators were located on the truss neutral axis in both bending directions at the 1/2 and 3/4 stations. These actuators were to provide additional control authority for the bending mode pairs.

2.5 Performance Measurement -- The design of active vibration control systems for future space structures will be driven by one of more system performance metrics such as line-of-sight (LOS) pointing error or surface shape error. A performance metric, when used in an optimal control design process, weights the contribution of individual structural modes in the controller to the overall system performance. Therefore, it was important in the design of the 12-Meter Truss Active Control Experiment to establish a performance metric or figure-of-merit to provide a realistic control design environment. It was also important that the metric used for control design could be easily measured in the experiment to assess actual controller performance.

For the experiment design process, the truss was considered dynamically representative of an appendage or boom supporting a precision sensor on a large space platform. The sensor would have an LOS pointing error figure-of-merit, so the LOS pointing error of a device mounted at the truss tip would make an acceptable figure-of-merit for the experiment. The LOS of a low power laser source mounted at the truss tip and pointing at a target array was considered first as a practical figure-of-merit that could be easily measured. Unfortunately, however, safety considerations at Wright Laboratory precluded the convenient use of such a laser. An alternative to an actual line-of-sight metric was to track the position (displacement) of a point at the truss tip in a plane perpendicular to the truss axis. If the point to be tracked was offset to one side of the truss axis, its position would include the effects of both bending and torsion modes with the offset distance affecting the torsion contribution. This approach was implemented in

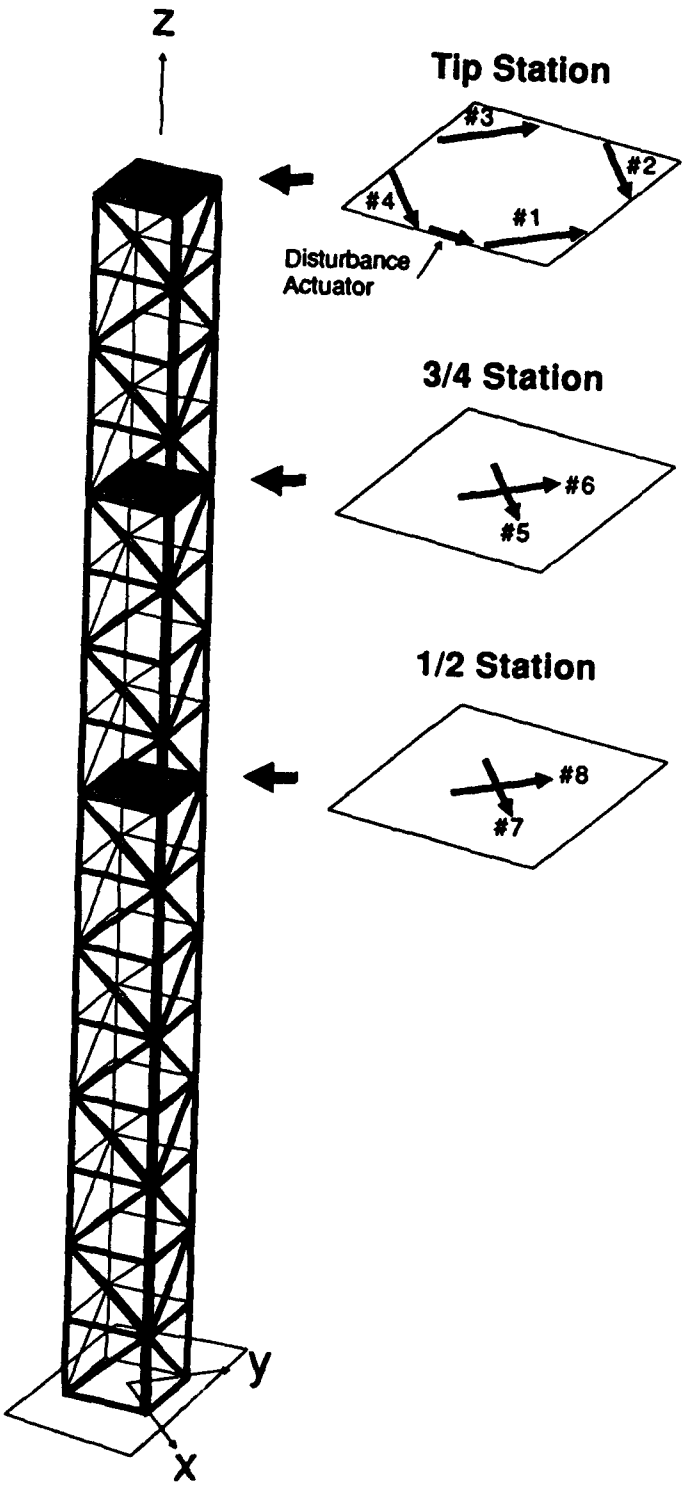

Figure 3. 12 Meter Truss Sensor and Actuator Locations

the experiment by mounting a small point light source at the truss tip offset to one side and measuring the planar position of the light source with a photodiode optical sensor mounted near the base of the truss. This approach is shown schematically in Figure 4 and is described in detail in Section 3.

The performance of a space structure is measured by the response of the figure-of-merit to disturbances, both internal and external. For this experiment, it was decided to apply a single point disturbance force at the truss tip which would excite all truss modes of interest. The disturbance force would be generated by an extra actuator at the truss tip oriented to excite both bending and torsion modes. A random force with a 50 Hz bandwidth was selected as the disturbance. This would excite modes in the control bandwidth and above it. In summary, the control figure-of-merit for the experiment was to minimize the displacement of the tip light source in the presence of a band-limited random disturbance applied to the truss tip.

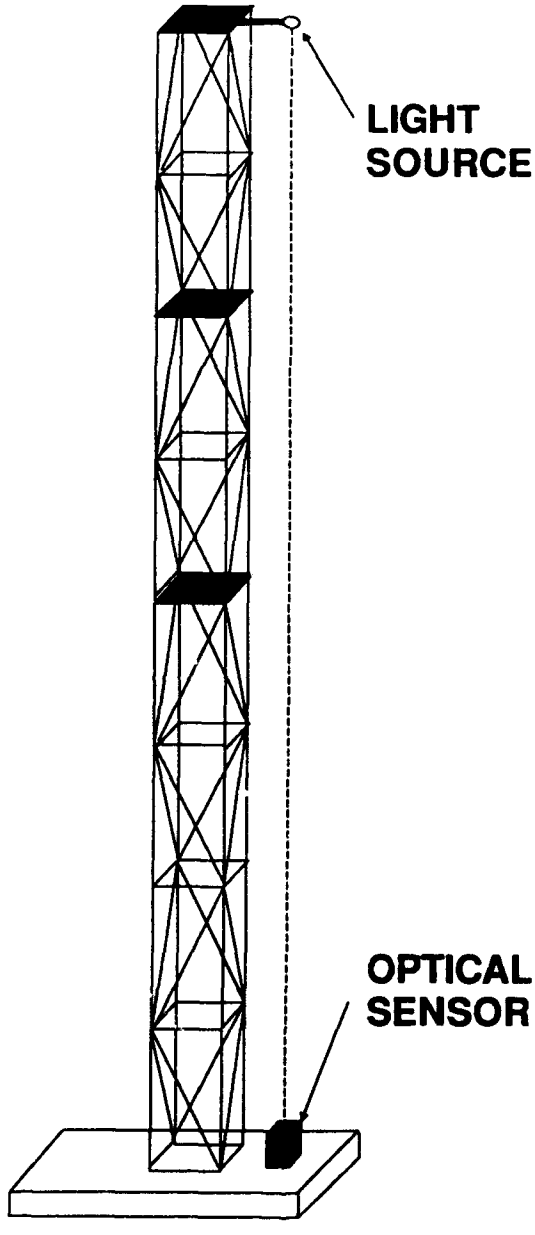

Figure 4. Truss Tip Position Sensing Configuration

3.0 HARDWARE DESCRIPTION

The physical configuration of the 12-Meter Truss Active Control Experiment is described in this section. The description includes the truss itself, accelerometers and analog integration circuitry, actuators and their power drivers, the tip position optical sensor and the real-time digital control computer.

3.1 Truss Description -- The basic structure of the experiment is the lightly damped 12-meter truss cantilevered vertically from a rigid base. The truss is assembled from four equal length frames of welded tubular aluminum alloy longerons and battens with bolt-in tubular Lexan diagonals in a back-to-back "K" pattern. The truss has a square cross section 20 inches on a side. The longerons are 6061-T6 aluminum alloy tubes with a 1.5-inch-square cross section and 0.065-inch wall thickness. The battens are 6061-T6 tubes with 0.50-inch square cross sections and 0.063-inch wall thickness. The diagonal members are Lexan tubing with a circular cross section of 1.50-inch diameter and have a 0.125-inch wall thickness. The diagonals have aluminum end fittings and are fastened to the truss frame with two bolts and a half-clevis joint at each end. The truss has 4 bays in each of the 4 sections for a total of 16 bays. The four sections bolt together with two bolts at each longeron. A single bay of the truss is shown in Figure 5. The base of the truss is securely bolted to the floor of the Vibration Test Facility (VTF) at Wright Laboratory. A scaffolding is located beside the truss to provide access to the sensors and actuators . The truss and scaffolding are shown in Figure 6.

3.2 Overall Control System Configuration -- The overall active control system for the experiment is shown schematically in Figure 7. The control system is made up of 8 sensors and signal conditioners, a 12-channel real-time digital control computer, and 8 actuators with power drivers and velocity feedback circuitry. Each accelerometer produces a signal proportional to the truss acceleration at its attachment point. The acceleration signal is integrated in analog circuitry to form a velocity signal which is fed to the control computer. The computer reads the vector of eight velocity signals and computes a vector of eight actuator command signals based on the control law being implemented. Each actuator command signal is fed to a current drive which powers the actuator and generates the desired control force. Each actuator is also equipped with a relative velocity sensor which is used with a variable gain amplifier to provide local velocity feedback damping to the actuator moving mass. An optical photodiode array sensor is used to track the motion of a small light source offset to one

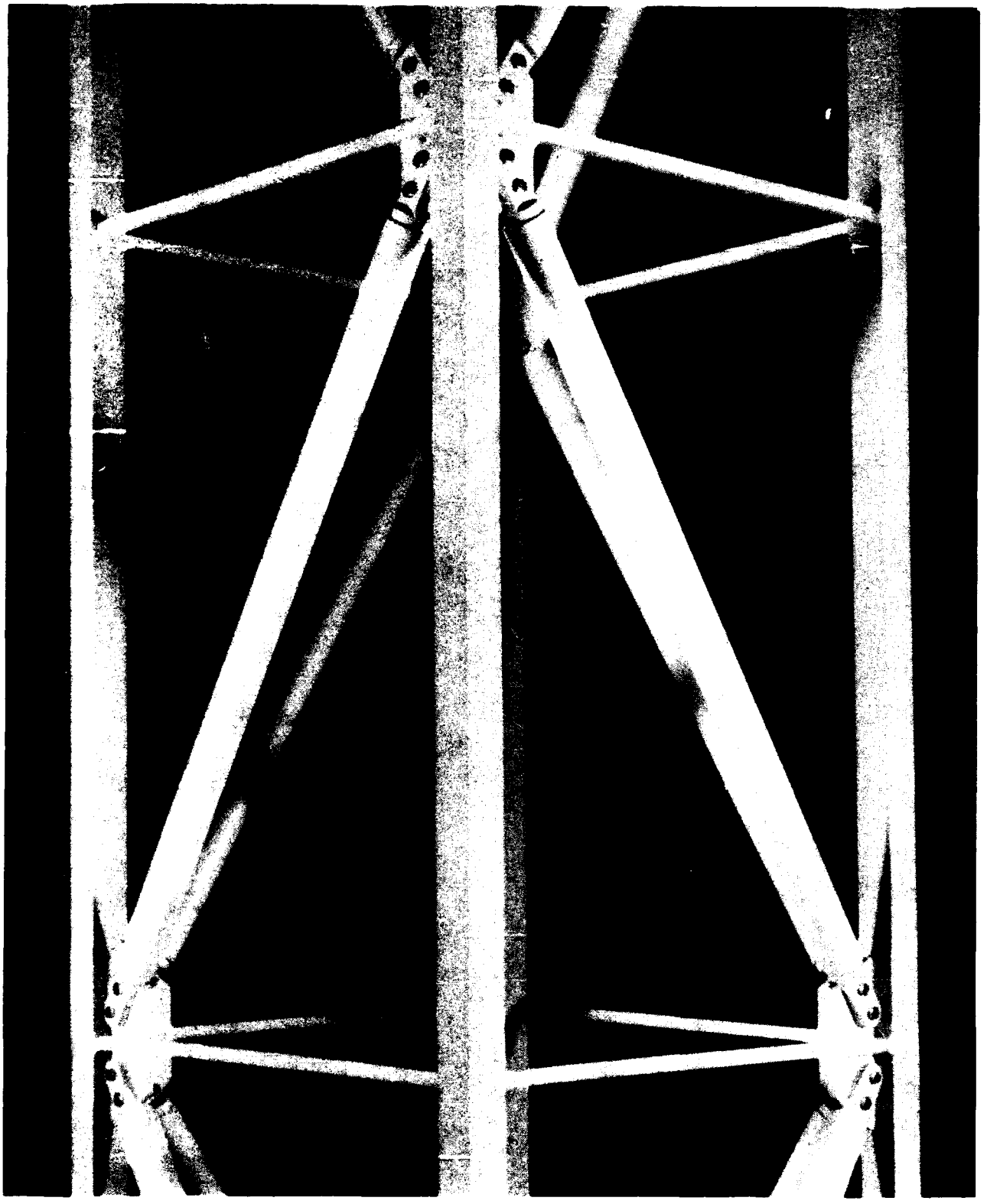

Figure 5. Single Bay of the Lightly Damped Truss

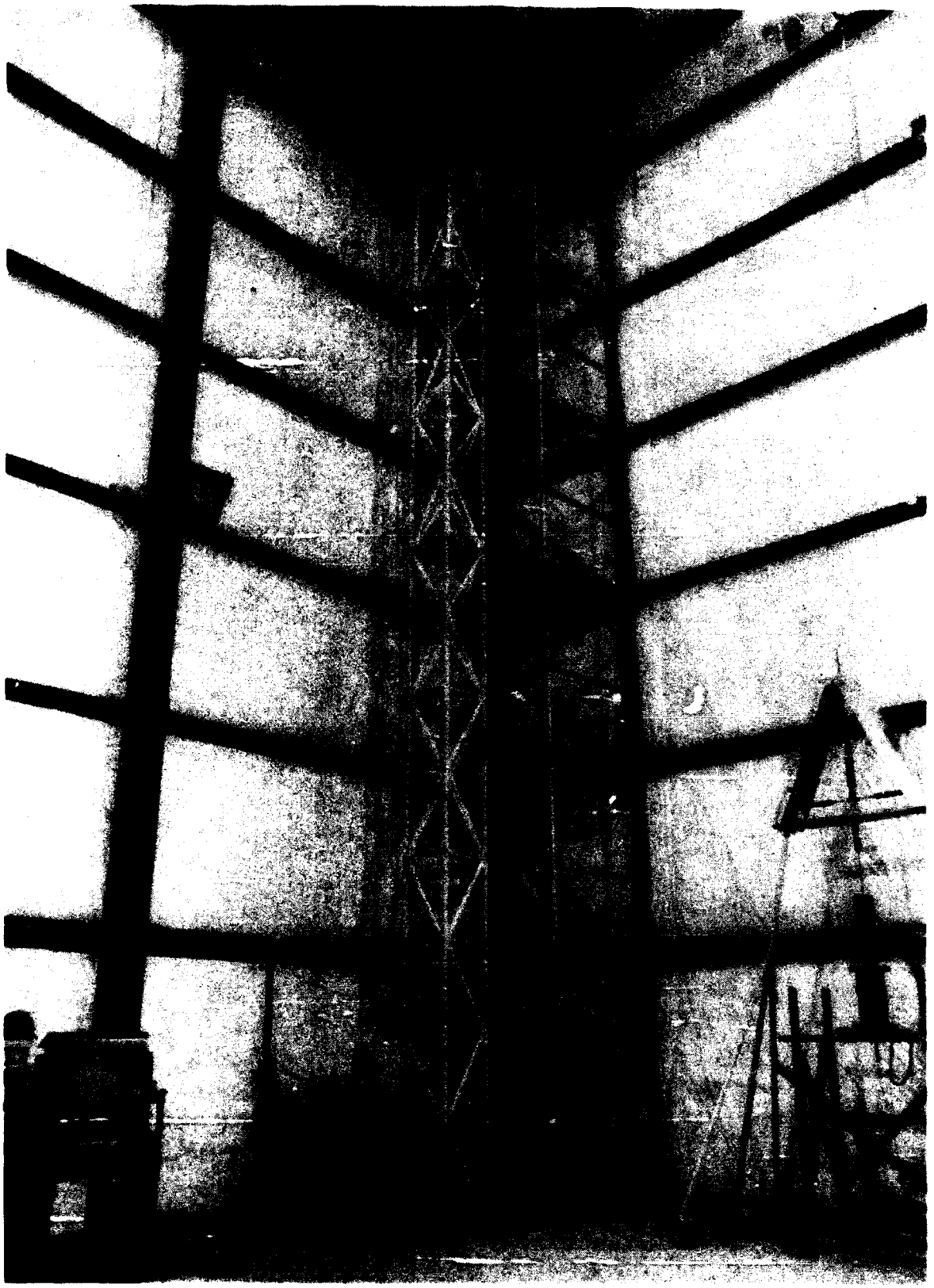

Figure 6. 12 Meter Truss Experiment in the Vibration Test Facility

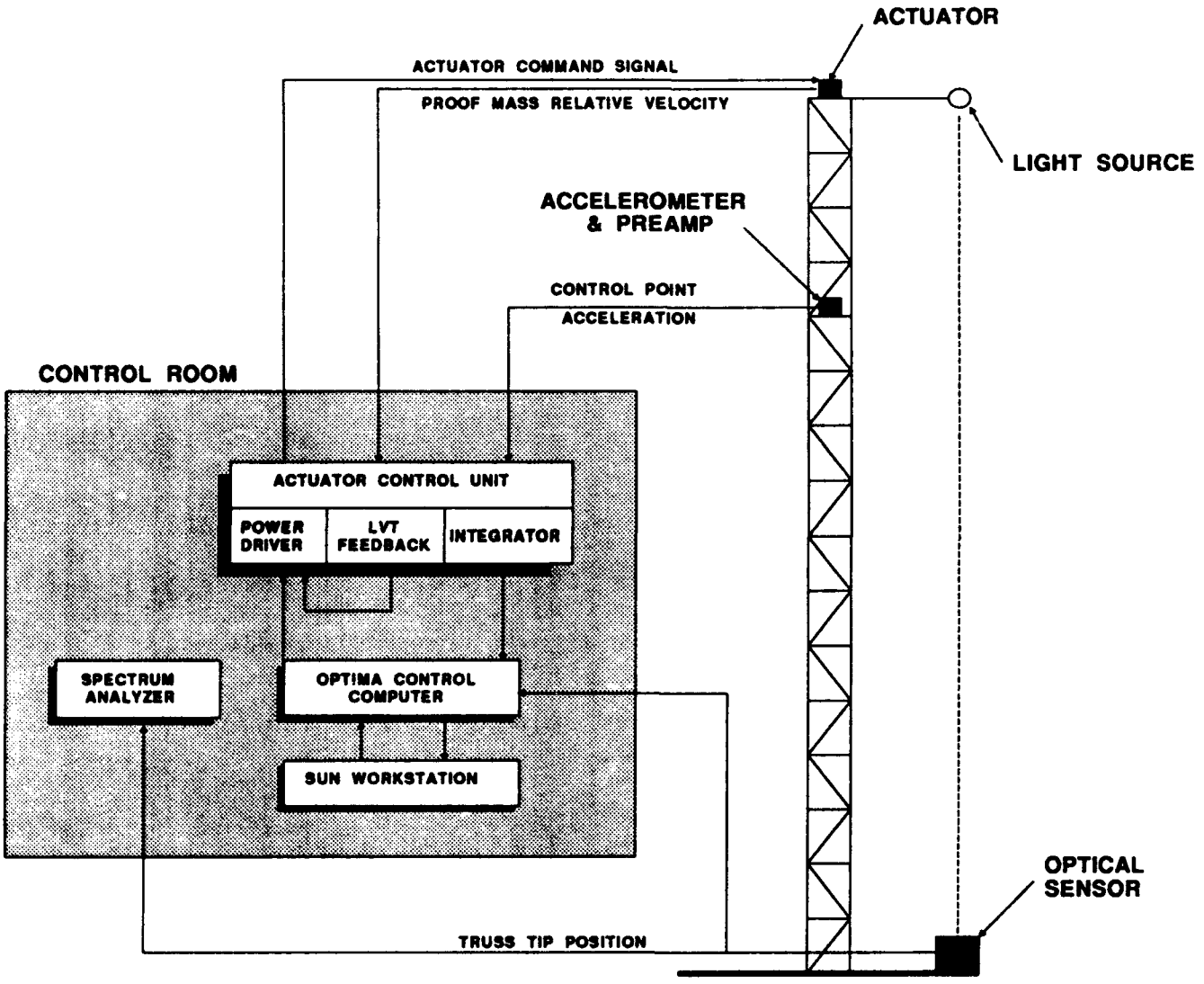

Figure 7. Overall Active Control System Configuration

side of the truss tip. The sensor produces signals proportional to the X and Y-axis displacements of the light source in a horizontal plane. The displacement signals are then input to the control computer and stored for off-line analysis of controller performance. Sensor inputs and actuator commands are also stored in the control computer for parameter identification and performance evaluation. In addition to control computations, the control computer is used to generate disturbance inputs to the truss and to control the overall timing of tests.

Disturbance forces are applied to the truss by an extra actuator and an electromagnetic shaker mounted at the truss tip. The disturbance actuator is aligned at a 45 degree angle with the truss bending axes and is offset approximately 8 inches from the truss axis so that it can excite all bending and torsion modes of interest with up to 1 pound of force. The shaker is mounted to the wall adjacent to the truss tip and is attached to the disturbance actuator housing. It can apply up to 10 pounds of force in the same location and direction as the actuator. Completing the control system is the real-time control computer which is connected to a Sun graphics workstation for control law development and simulation, downloading code to the control computer, uploading experimental results and analysis of measured data.

3.3 Sensors -- The experiment uses eight piezoelectric accelerometers to sense motion for active feedback control. Each accelerometer is mounted to the housing of one of the control actuators and senses motion along the actuator axis. The measured acceleration signal is converted to velocity by an analog bi-quad integrator circuit. All circuitry used for sensor and actuator signal conditioning was derived from designs used by Martin Marietta on the PACOSS contract [3]. An ideal integrator circuit is not desirable since it has infinite gain at dc which amplifies any dc bias which may be on the acceleration signal. The bi-quad integrator circuit used by Martin behaves as an ideal integrator above some break frequency, but below the break it behaves as an ideal differentiator with very low gain at dc The break frequency was set at 0.1 Hz for the truss experiment which is more than 1 order of magnitude below the lowest frequency of the truss. This resulted in generally good integrator performance over the entire control bandwidth of the experiment with essentially zero gain at dc However, a relatively high level of noise was present in the integrated acceleration signals at the break frequency. This noise was simply accelerometer noise being amplified by the high gain of the integrator at the break frequency. The noise appeared as a low frequency drift on the velocity signal which was passed through the control computer and superimposed on the

actuator command. The integrated accelerometer signal is also amplified by a variable gain. The gain is used to increase the velocity signal level for better signal-to-noise ratio in the control computer analog input.

3.4 Actuators -- Control forces for the truss are provided by eight linear momentum exchange (proof mass) type actuators capable of approximately 1-pound-force peak output. Each actuator is equipped with a moving mass relative velocity feedback circuit for adding damping to the actuator response. Power is provided to the actuators by individual current drive circuits.

The 12-meter truss actuator uses a linear dc motor with the armature fixed to a base and the permanent magnet field suspended on shafts and linear bearings. The actuator is shown in Figure 8. The design is a modified version of the Martin PACOSS actuator, shown in Figure 2. The same linear dc motor and drive circuitry are used, but the shaft, bearings and centering spring arrangement are different. The PACOSS design employed a single shaft through the center of the linear motor permanent magnet which was known to significantly reduce motor force output. To eliminate this problem, dual shafts were positioned on either side of the moving mass. This approach does, however, increase the friction force acting on the moving mass. Available moving mass travel is 1 inch on either side of the equilibrium position. The PACOSS actuator was designed for use in a vertical configuration so the centering springs also had to support the weight of the moving mass. The truss application called for a horizontal layout so the centering springs were modified to provide the necessary centering force only. The truss actuator uses a linear velocity transducer (LVT) to sense the relative velocity between the moving mass and the actuator base. The relative velocity signal is amplified with a variable gain and fed back to the motor to provide an equivalent viscous damping for the moving mass. The LVT feedback damping implementation is identical to the PACOSS design. The PACOSS current drive design is also used without modification and provides a force constant of approximately 0.1 pound per volt. The four control actuators and the disturbance actuator at the truss tip station are shown in Figure 9. The truss control actuators at the 1/2 station are shown in Figure 10.

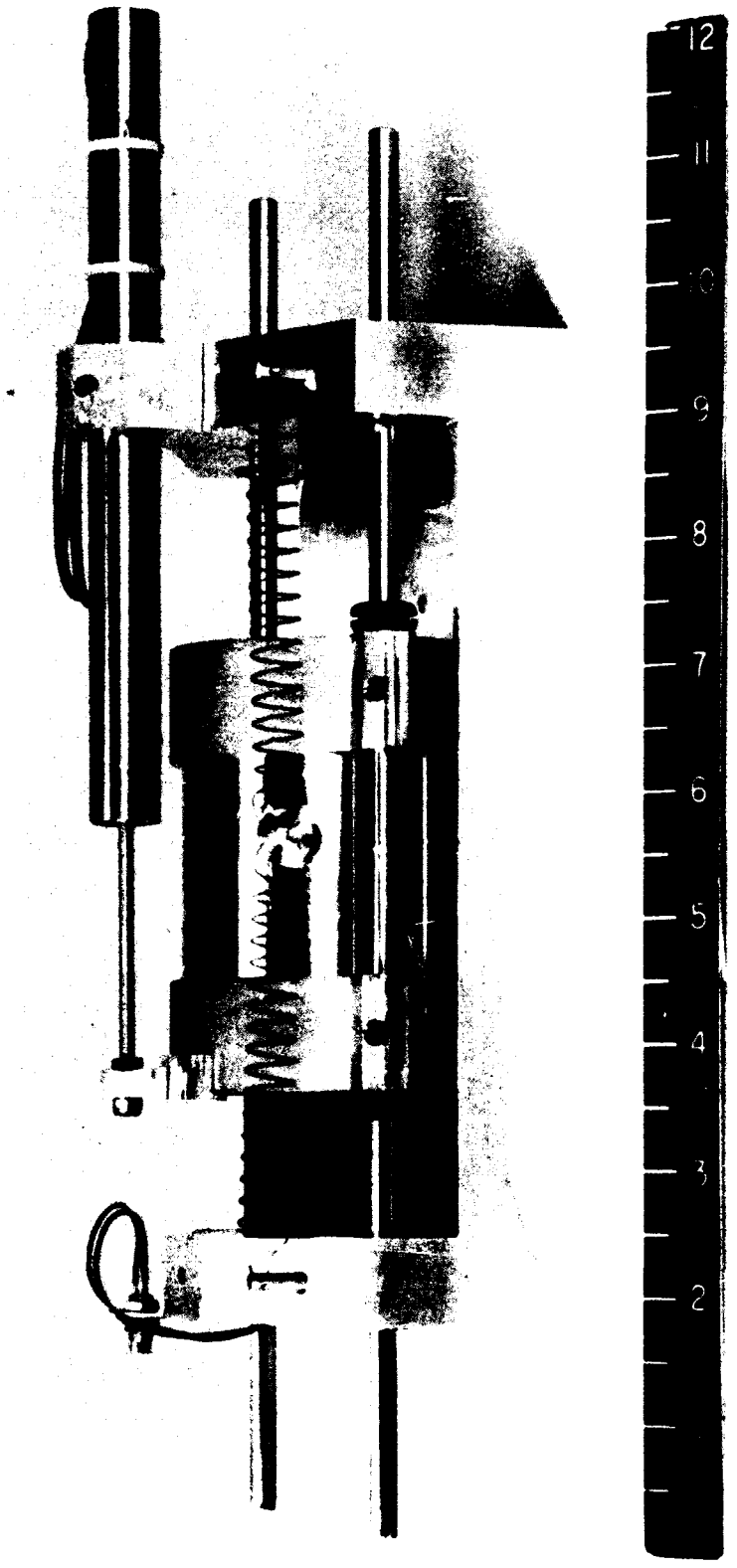

Figure 8. 12 Meter Truss Actuator

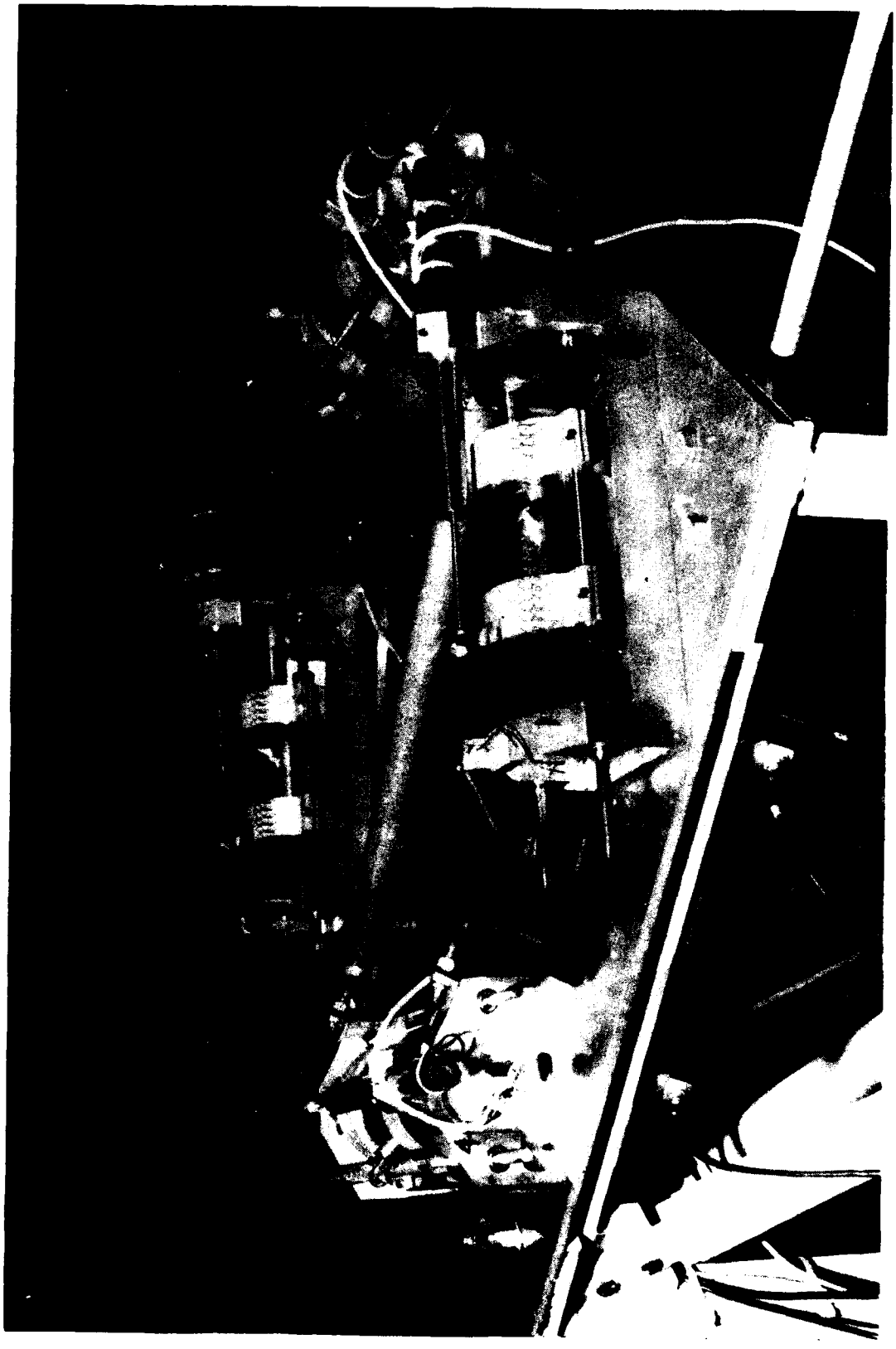

Figure 9. 12 Meter Truss Tip Station Actuators

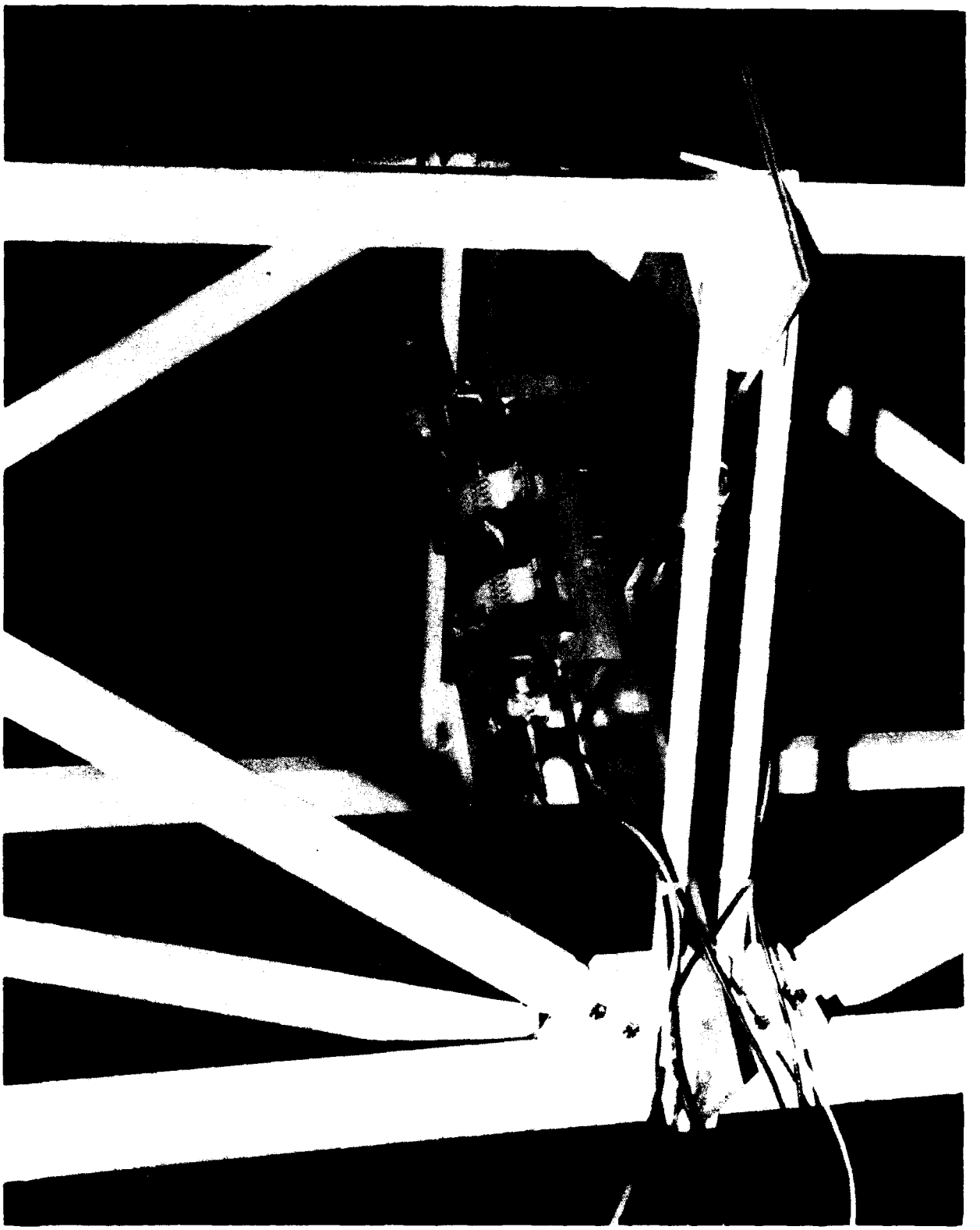

Figure 10. 12 Meter Truss 1/2 Station Actuators

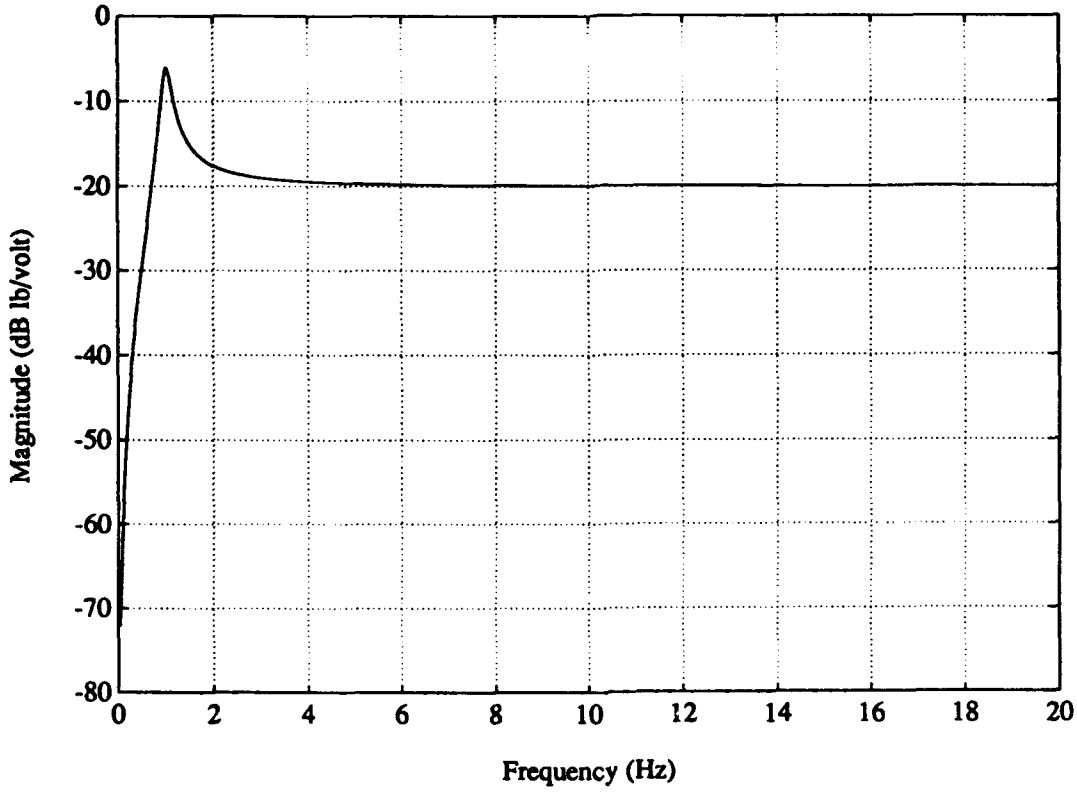

Figure 11. Actuator SDOF Model Transfer Function

Before the actuator design could be "tuned" for the truss application it was modelling as a single degree-of-freedom (SDOF) system with the relative velocity feedback providing an equivalent viscous damping. The transfer function, H_{act}, of the SDOF actuator model output force to commanded input voltage can be expressed as

$$H_{act} = C_m \frac{\omega_n^2}{\omega_n^2 - \omega^2 + j\,2\,\zeta\,\omega} \qquad (1)$$

where C_m is the actuator and drive circuit gain, ω_n is the actuator natural frequency in radians per second, ζ is the actuator damping ratio and ω is drive frequency in radians per second. The magnitude of H_{act} from equation (1) is plotted versus frequency in Figure 11 for an actuator damping ratio, ζ, of 10%. As can be seen in Figure 11, the transfer function gain is constant at frequencies significantly above the actuator resonant frequency. This is a desirable feature for active control since the actuator can be treated as a constant gain device in this frequency region and no actuator dynamics need to be included in the design model.

The initial plan to tune the actuator was simple; the centering spring stiffness would be adjusted to provide an actuator resonant frequency significantly below the lowest truss mode and as much damping as possible would be added to suppress moving mass resonant response. Unfortunately, this approach worked less well in practice. First, the centering spring stiffness was adjusted to achieve an actuator resonant frequency of 1 Hz, or 50% of the predicted 2-Hz fundamental bending mode frequency. For this value of spring stiffness, the centering forces for small displacements about the moving mass equilibrium position were on the order of the shaft friction forces. So, 1 Hz was a practical lower limit for the actuator resonant frequency. But, with a 1-Hz actuator resonance, the transfer function magnitude and phase at the first truss mode frequency were significantly different from the desired values for both the 10% and 50% damping cases. Thus, it was decided to abandon the constant gain actuator approach and include actuator dynamics in the design model. This approach had the added benefit of providing a more accurate system model due to the significant coupling of the actuator moving masses to the truss modes at low frequencies which was not accounted for by a constant gain actuator model. In summary, the actuator design configuration was selected with a 1-Hz resonant frequency and damping ratio of 10% of critical. Higher values of damping ratio would be used if actuator mode stability became a problem.

A prototype actuator was fabricated to verify the final design. The prototype was tested to measure its natural frequency and damping ratio and to verify the accuracy of the SDOF model. First, the transfer function between force output and voltage command to the current drive was measured in a frequency range of 0-100 Hz, with LVT feedback damping turned off, using a sine sweep test method. Output force was computed from the measured acceleration of the moving mass. A resonant frequency of 0.91 Hz was identified from the transfer function. This was somewhat lower than the design value of 1.0 Hz and was probably caused by the stiffness of the return springs being less than the design value. A nominal damping ratio of 0.064 was measured using the log decrement method on a free decay time history of the moving mass relative velocity. The LVT feedback was then turned on and the gain adjusted to give a damping ratio of 0.10 as measured by log decrement. The transfer function was again measured, this time with 10% LVT damping and compared to the SDOF model. The agreement with the model was acceptable.

Later in the project the transfer function of one of the actuators was measured as

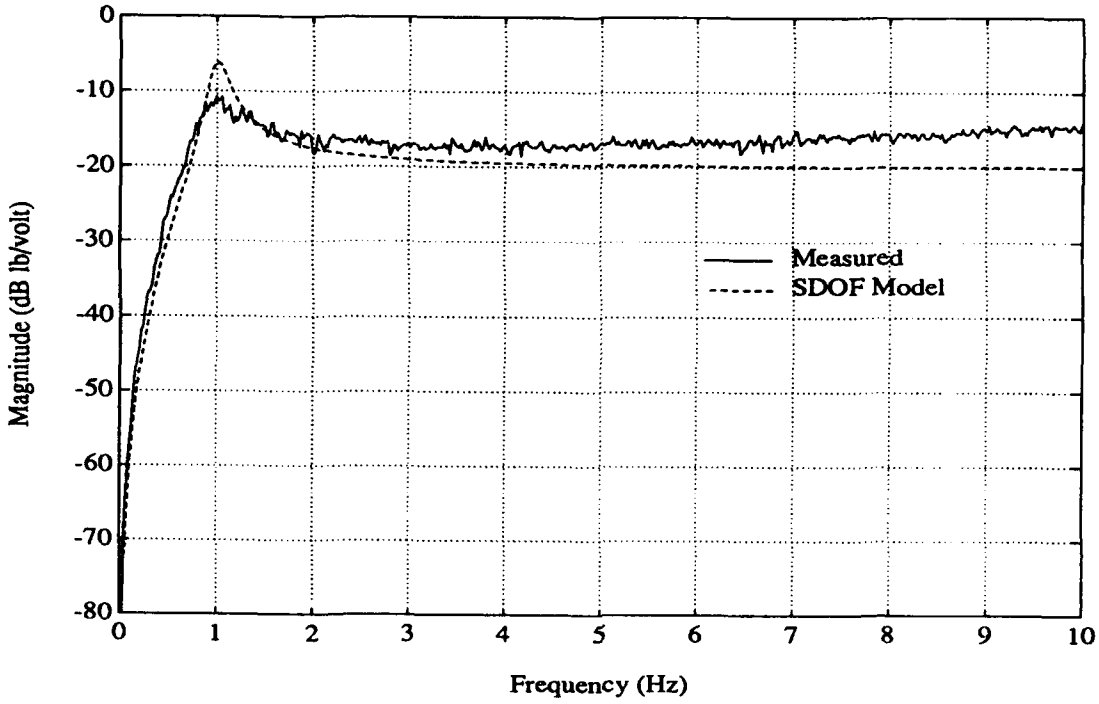

Figure 12. Measured and SDOF Model Actuator Transfer Functions

part of an effort to better characterize the sensors and actuators. The transfer function is shown in Figure 12 with the SDOF model. It is apparent from the figure that the actuator damping is appreciably higher than the model and that the nominal gain is also higher than the model. The increased damping may be due in part to the random input test method used to measure the transfer function. The effective damping from the Coulomb friction force in the actuator increases with decreasing response amplitude. Since the random test produces considerably less response amplitude in the actuator than the original sine dwell test did, the damping could be expected to be higher. The increased damping may also have been caused by wear in the actuator shafts and bearings which could result in higher friction forces. The difference in transfer function magnitude is due to errors in the initial characterization of the actuator.

The actuator design was judged acceptable based on the prototype testing and the remaining seven actuators were fabricated. The nominal damping of the actuator mode was first measured with no LVT feedback and with the LVT rod disconnected using the log decrement method. Measured values ranged from approximately 5% to 7% of critical. Next, the damping was measured with the LVT rod connected but with no

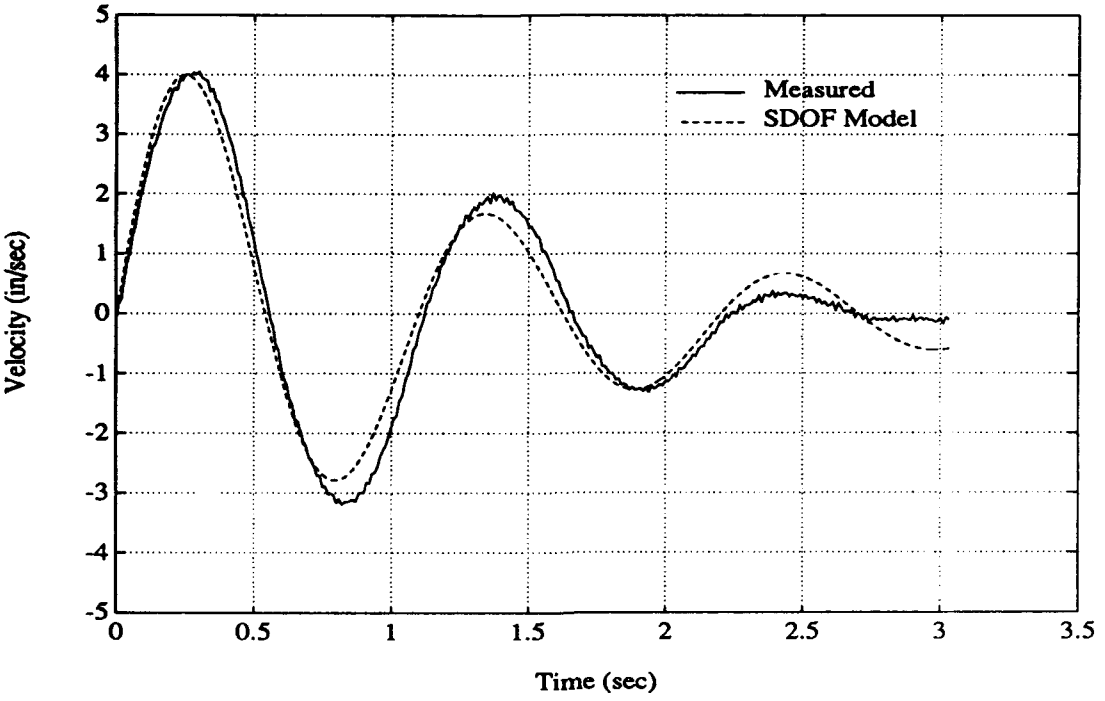

Figure 13. Typical Actuator Free Decay Response with Viscous Envelope

feedback. The measured values increased to the 7% to 10% range. Finally, the LVT feedback damping was turned on and the gain adjusted for each actuator to achieve a 10% damping value. The level of LVT feedback gain required was small since all of the actuators had damping values near 10% without LVT feedback. The gain setting for 50% damping was calculated by linearly extrapolating from the 10% value.

The free decay damping measurements of the actuators were based on a linear viscous damping model inherent to the log decrement method. Actually, the damping behavior exhibited by the actuators was not purely viscous. This subject was investigated in some detail after the initial open-loop testing of the truss in an attempt to explain the higher than predicted modal damping values measured for the first bending mode pair. The deviation from purely viscous damping can be seen in Figure 13 where a typical actuator decay trace (without LVT feedback) is shown with a viscous damping model as identified by the method of Agneni and Balis Crema [5]. It seemed logical that the primary source of damping in the actuator was Coulomb (sliding) friction of the actuator shafts and bearings, not viscous damping. Pure Coulomb friction damping produces a linear decay envelope [6], however, so the actuator response as shown in Figure 13 is not

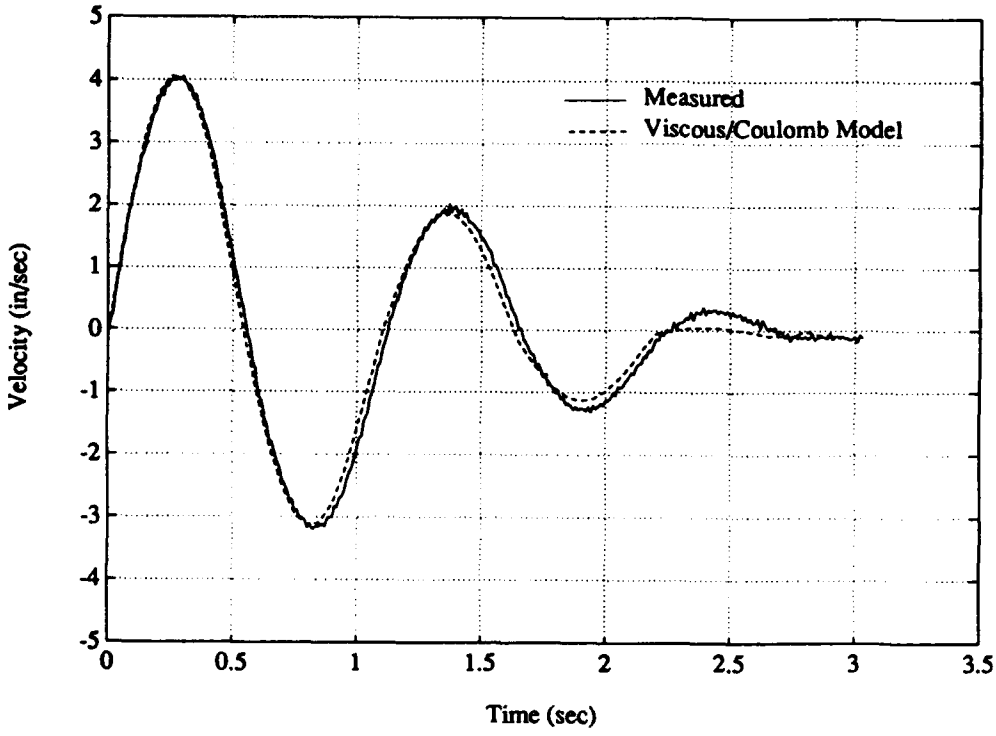

Figure 14. Typical Actuator Free Decay Response with Friction-Viscous Model Envelope

due solely to friction either.

At this point, a method was developed to identify both viscous and Coulomb friction damping contributions in the actuator response. This method was able to identify the friction effects, the viscous effect of the LVT feedback damping and additional viscous damping, the source of which was unknown. The possibility of contributions from other damping mechanisms was considered, but was not pursued due to the good results obtained with the Coulomb friction-viscous damping model. The identification approach used resonant dwell test data to fit a SDOF model with an equivalent viscous damping coefficient including both viscous and Coulomb friction effects. The model results in a linear relationship between the steady state displacement amplitude, X, of the model at resonance and the driving force amplitude, F, which is given by

$$X = \frac{1}{2\,\zeta\,K}\,F - \frac{2\,F_c}{\pi\,\zeta\,K} \qquad (2)$$

where ζ is the viscous damping ratio, F_c is the Coulomb friction force and K is the system stiffness. Development of the combined damping model is presented in detail in [7]. Typical results of this identification approach are shown in Figure 14. The figure

Table 2. Viscous Damping Ratios and Coulomb Friction Forces in the 12-Meter Truss Actuators

Actuator No.	Frequency (Hz)	Damping Ratio[1]	Friction Force[1] (lb)	Effective Damping[2] Ratio
1	0.91	0.046	0.017	0.104
2	"	0.024	0.041	0.242
3	"	0.040	0.020	-
4	"	0.060	0.016	-
5	"	0.059	0.012	-
6	"	0.068	0.032	-
7	"	0.046	0.032	-
8	"	0.050	0.025	-

[1] Measured by the resonant dwell method

[2] Measured by viscous fit to free decay data

shows the free decay response of an actuator without LVT feedback plotted with the response predicted by the combined damping model. The agreement is better than the viscous model shown in Figure 13.

The combined damping model was used to characterize all eight truss actuators. The testing was done with the actuators mounted on the truss. Comparison of test results of an actuator on the truss to one on a fixed base showed a negligible effect of coupling on truss mounted actuator frequencies. Table 2 lists the resulting values of Coulomb friction force and viscous damping ratio for each actuator. The viscous damping ratios shown in the table range from 2.4% to 6.8% of critical. It is not clear what the source of this damping is or whether it is truly viscous damping and not an approximation of some other damping mechanism. The friction forces shown in the table are quite small in absolute terms but have a significant effect on actuator response. The effective viscous damping ratio obtained by fitting a purely viscous model to the data is also listed in the table for actuators 1 and 2. Note that the effective viscous damping ratio of actuator 2 is over 24% while it was measured at less than 10% when the actuator was new. The

effect of the friction force can be seen in the difference between the viscous damping ratio identified from the combination fit and that from the purely viscous fit. For example, the friction force of 0.041 pound measured for actuator 2 increases the viscous damping from 2.4% to 24.2%; a very large increase. It should be noted that the effective viscous damping contribution of a Coulomb friction force is linearly dependent on the response amplitude and frequency [6], but this comparison still illustrates the significant effect of friction on actuator response.

3.5 Tip Position Optical Sensor -- The 12-Meter Truss Active Control Experiment used the position of a small light source offset to one side of the truss tip as a figure-of-merit for active control performance measurement. The light source position was measured by a 2-dimensional optical sensor mounted near the base of the truss. The rationale for selecting the light source configuration was discussed in Section 2.5.

The general arrangement of the light source and optical sensor is illustrated in Figure 4. The light source is a 12-volt-dc light bulb supported by an aluminum tube at a distance of 24 inches from the truss axis. The position of the light source in a horizontal plane is monitored by a photodiode optical sensor mounted on the facility floor directly below the light source. The optical sensor, developed at Wright Laboratory, is based on a lateral-effect photodiode sensing element which is mounted at the focal plane of a 35-mm single lens reflex camera. A 1000-mm telephoto lens is used with the camera body to provide a magnification of the motion of the light source image on the sensor element. The sensor element and its signal conditioning electronics produce a continuous voltage proportional to the distance between the centroid of the imaged light spot on the element and the geometric center of the element. The sensor system has a resolution of 1 part in 1000 in each measurement axis. The resulting absolute sensitivity of the sensor and lens combination is approximately 1.2 volts of signal output per inch of light source displacement in either axis. The two orthogonal sensor axis output signals were sampled and stored in the real-time control computer for control performance measurement. The optical sensor is shown in Figure 15.

3.6 Real-Time Control Computer -- A Systolic Systems Optima 3 real-time control computer was used to implement active control approaches, acquire data for open-loop tests and provide overall control of the experiment. The Optima 3 system, shown schematically in Figure 16, consists of two major components; the development system and the real-time controller. The development system, a Sun Microsystems

graphics workstation, is used for software development, simulation, downloading of control code to the controller and analysis of test data. The real-time controller is a VME-based computer with a fast host processor, 12 channels of 16-bit, single-ended analog input and output, a high speed vector processor and 4 Mbytes of memory for code and data storage. The controller provides the real-time control code execution as well as data acquisition and disturbance signal generation. The controller is fully programmable in the C language which allows a wide range of nonlinear or time varying control laws with concurrent sampling and storage of desired time histories. The Optima system was used for all open-loop testing of the experiment including sine sweeps, continuous random and free decay tests. Dynamic data were acquired and stored on the controller and then uploaded to the development system for analysis using the Matlab software package.

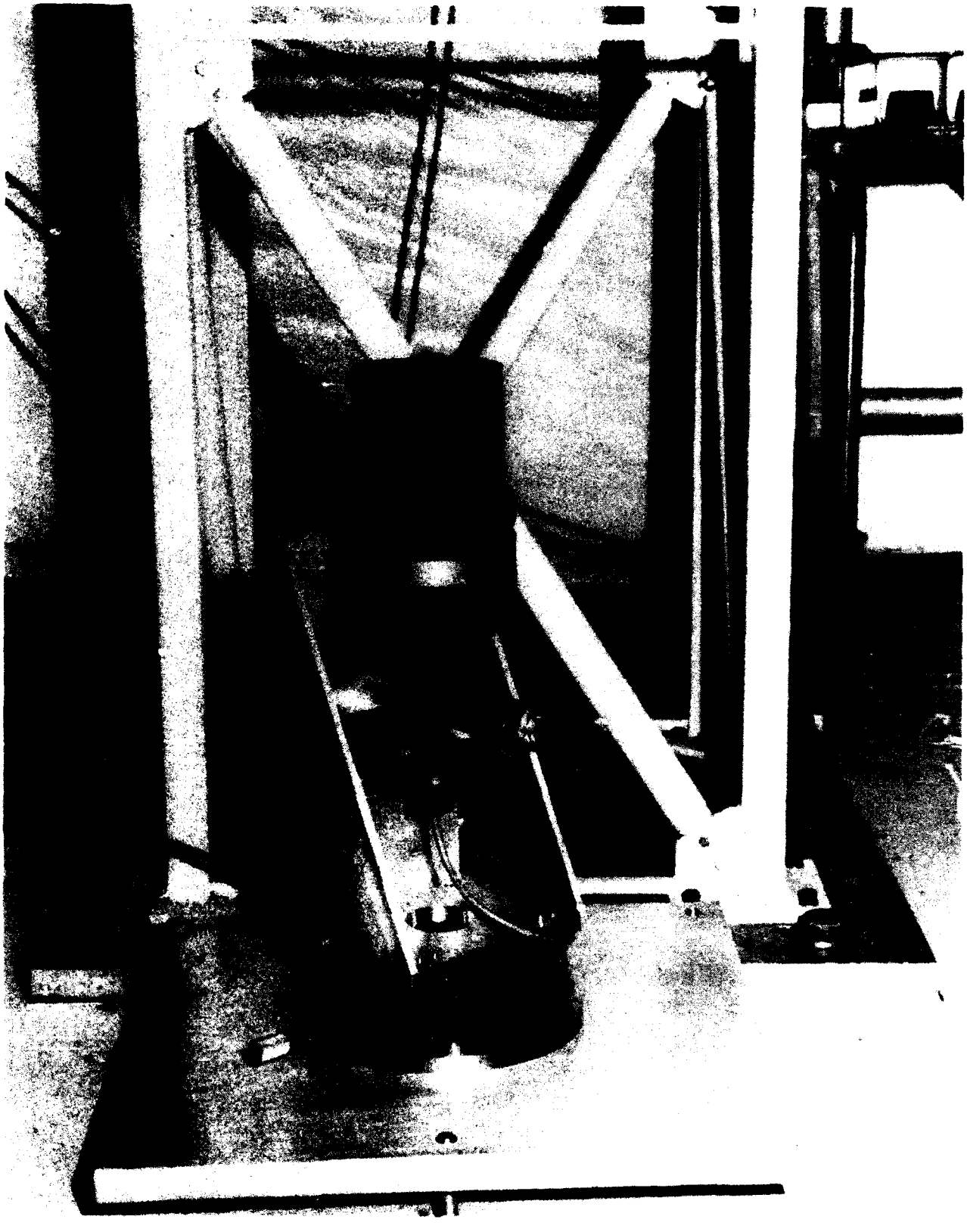

Figure 15. Truss Tip Figure-of-Merit Optical Sensor

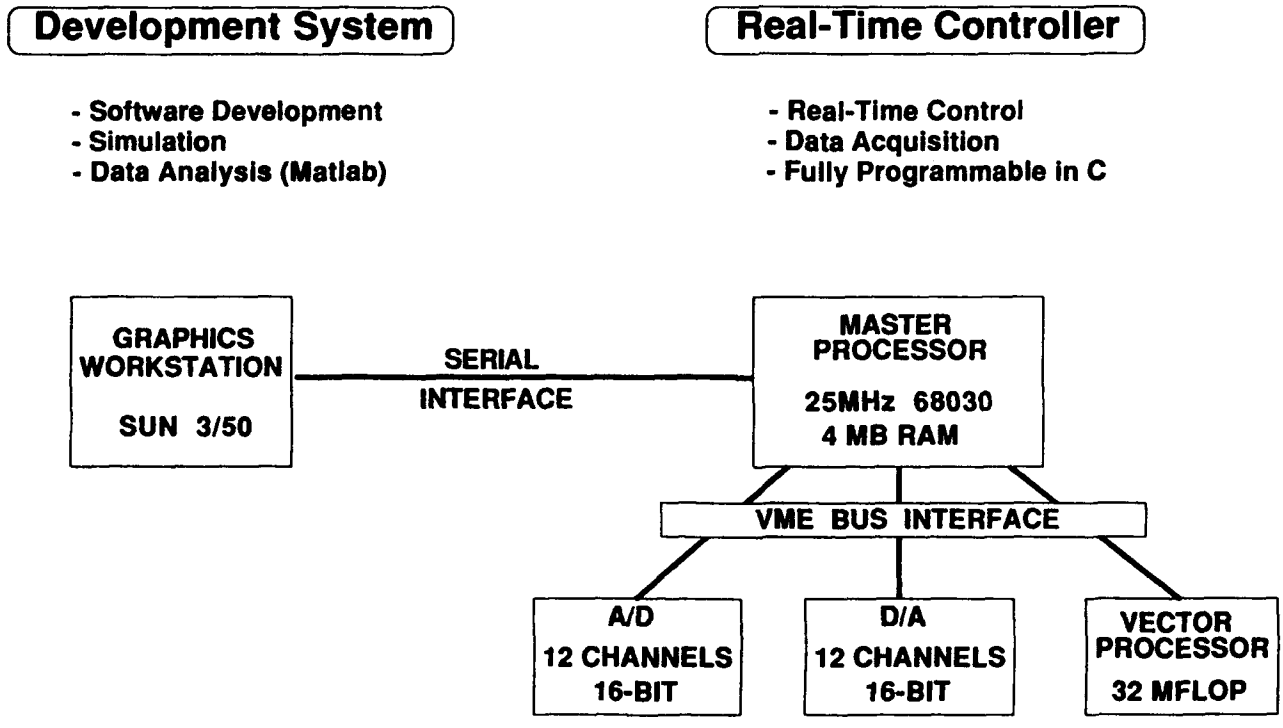

Figure 16. Optima Real-Time Control Computer

4.0 DYNAMIC ANALYSIS OF OPEN-LOOP SYSTEM

The 12-meter truss with active control hardware was modelled using the finite element method to predict open-loop system response. Both a frame model and an equivalent continuous beam model were developed. The finite element models were also used to generate a reduced order state space model for active control design and simulation.

4.1 Truss Finite Element Model -- A finite element model of the lightly damped 12-meter truss was developed prior to the active control experiment to predict dynamic properties for comparison with test results. This model, which represented the truss as a frame structure, was modified to include control actuator dynamics and support structure for this experiment. The model was developed and analyzed using MSC PAL2 finite element software on a personal computer. Each truss member was modelled as a beam element with 6 degrees of freedom (DOF) at each node. The four nodes at the truss base were fixed to simulate the cantilever boundary condition. The truss model had a total of 192 beam elements and 384 active DOF.

The eight control actuators were included in the truss model as SDOF spring-mass-damper systems with 1.0 Hz resonant frequencies and 10% modal viscous damping. The disturbance actuator, mounted at the truss tip at a 45-degree angle to both truss bending axes, was modelled as a pair of actuators. They were aligned with the bending axes and had the same resonant frequency as the real actuator but with moving mass and spring stiffness values of 0.707 times their actual value. Thus, there was a total of 10 actuators in the model, but the dynamic effect was that of the actual 9. With actuators, the frame model had over 440 active DOF.

The frequencies predicted by the original model of the undamped cantilevered truss did not agree very well with measured values. The frequencies of the lowest eight flexible modes of the original model are listed in Table 3 along with the measured values. The model over-predicted the first X and Y-axis bending frequencies by 10% while it under-predicted the first torsion frequency by about the same amount. The agreement for the higher bending modes is somewhat better. Attempts were made to correct the model to obtain better agreement with test frequencies. The goal was to have the model agree with the measured first bending and torsion frequencies, within 1%. The attempts included adjusting the elastic moduli (and therefore the axial stiffnesses) of the

Table 3. Predicted and Measured Frequencies of the Undamped 12-Meter Truss - Cantilevered

	Truss Frequencies (Hz)		
Mode	Measured	Predicted	Error (%)
1st X Bending	2.26	2.48	9.5
1st Y Bending	2.25	2.50	10.9
1st Torsion	7.10	6.34	-10.8
2nd X Bending	10.72	10.90	1.7
2nd Y Bending	10.72	11.00	2.6
2nd Torsion	21.27	19.04	-10.5

longerons and diagonal members and modelling the base boundary condition with stiff springs. All of these parameters had significant effects on truss frequencies, but it was not clear what combination of adjustments was optimal and physically plausible. To eliminate the effects of the base boundary condition, the model was also compared to test results from the truss mounted horizontally on a soft suspension simulating free boundary conditions. The results of this comparison are shown in Table 4. Like the cantilever results, the free-free frequencies predicted by the model are high for bending and low for torsion. This indicated that the model itself was in error, not just the modelling of the cantilever boundary condition. Tuning of the free-free model was also attempted by adjusting the longeron and diagonal member stiffnesses. But, again, it was not possible to find a physically meaningful combination of parameters that corrected both the first bending and first torsion modes.

The problem with tuning both bending and torsion frequencies to match the model was that the torsional stiffness of the truss could not be varied independently. Changes in longeron stiffness affected only the bending frequencies, but due to geometry, changes in diagonal member stiffness affected both torsion and bending. To solve this problem the truss was modelled as an equivalent continuous beam with uncoupled bending and torsional stiffnesses. This allowed independent adjustment of

Table 4. Predicted and Measured Frequencies of theUndamped 12-Meter Truss - Free-Free

Truss Frequencies (Hz)			
Mode	Measured	Predicted	Error (%)
1st Y Bending[1]	12.65	13.55	7.1
1st Torsion	14.10	12.48	-11.5
2nd Y Bending	25.34	26.47	4.5
2nd Torsion	27.83	24.99	-10.2
3rd Y Bending	36.84	38.65	4.9

[1] X-axis bending modes are not included. They were not accurately identified due to coupling with the suspension

bending and torsion frequencies. In addition, the beam model was less complex and thus required considerably less computation time on the personal computer used for analysis.

4.2 Equivalent Beam Finite Element Model -- An equivalent continuous beam finite element model of the 12-meter truss was developed. This beam model was used to predict open-loop performance and generate a detailed control model of the control configured truss.

Each of the 16 bays of the truss was modelled as a single beam element. Beam element properties were computed by applying unit axial, bending, torsion and shear loads to a detailed model of a single truss bay. The beam element provided in the PAL2 software allows for independent adjustment of the effective shear areas of the element to account for shear deformation. Appropriate mass properties were added to the element. The beam elements were then "stacked" in an alternating pattern to capture the orthotropic properties of the truss element geometry. The beam model had 16 elements and 96 DOF including the 6 DOF at the truss base which were fixed for the cantilever boundary condition. Frequencies computed from the initial beam model with cantilevered boundary conditions are compared to values from the frame model in Table 5. Measured frequencies are also shown in the table. The beam model frequencies agree well with the frame model but are slightly higher for both bending and torsion.

Table 5. Predicted and Measured Frequencies of the12-Meter Truss Frame and Beam Models

	Truss Frequencies (Hz)			
Mode	Test	Frame	Initial Beam	Corrected Beam
1st X Bending	2.26	2.48	2.53	2.18
1st Y Bending	2.25	2.50	2.53	2.18
1st Torsion	7.10	6.34	6.52	7.17
2nd X Bending	10.72	10.90	11.11	10.23
2nd Y Bending	10.72	11.00	11.14	10.25
2nd Torsion	21.27	19.04	19.64	21.59
3rd X Bending	23.25	23.37	23.80	22.49
3rd Y Bending	22.98	23.54	23.85	22.54

The beam model with free boundary conditions was "tuned" to match the measured first bending and torsion frequencies of the free-free truss. Tuning of the first bending mode was achieved by adjusting the beam material elastic modulus while the element torsional stiffness parameter was adjusted to tune the first torsion mode. The elastic modulus was decreased by 30% and the torsional stiffness increased by 21% to force the model to agree with the test results. The frequencies for the tuned beam model with cantilever boundary conditions are shown in Table 5. Agreement with test results for all modes through third bending is very good. The physical explanation of why such large changes in bending and torsion parameters were necessary is not clear. However, since the model was used for performance prediction, not design modification, the need for physical correlation was secondary. Actuators were modelled as spring-mass-damper systems attached to the beam model in the same way as for the frame model of the truss. The beam model with actuators had 136 active DOF, considerably fewer than the 440 DOF for the frame model.

4.3 Open-Loop Dynamic Characteristics -- The equivalent continuous beam finite element model was used to predict open-loop frequencies and damping ratios for

the experiment. Frequencies and damping ratios were identified using the circle fit method [8] applied to transfer functions between sensor output velocities and actuator input forces. Damping ratios were also identified using the half-power bandwidth method on transfer functions. Transfer functions were computed for inputs at the disturbance actuator and actuator 5, an X-axis actuator at the 3/4 station of the truss. A typical transfer function between sensor 1, a Y-axis sensor at the truss tip, and the disturbance actuator is shown in Figure 17. Table 6 lists the frequencies and damping ratios predicted by the model for the first 17 modes of the truss. The first nine modes shown in the table occur at 1 Hz and are actuator modes. The first pair of X and Y-axis bending modes show up at 1.74 and 1.75 Hz, respectively. All of the bending modes occur in pairs that are very closely spaced in frequency but are not repeated modes. This is due to a slight difference in the stiffnesses in the two primary bending directions caused by truss geometry. The individual bending mode pairs are effectively uncoupled, despite their close frequencies, due to the nearly symmetric stiffness and mass characteristics of the truss. The first pair of bending frequencies is considerably lower than those for the bare truss, as shown in Table 1. This is to be expected since more than 74 pounds of actuators and mounting plates were added to the truss. Next in frequency comes the first torsion mode followed by the second and third bending pairs and then second torsion. These modes are also lower in frequency than those for the bare truss with the bending modes showing a larger reduction than the torsion modes.

Damping ratios identified for the truss modes are also shown in Table 6. Damping was included in the finite element model in two forms. The primary source of damping in the model was the LVT feedback in the actuators which was modelled with discrete viscous dampers. In addition to the LVT feedback, a small amount of proportional damping was added in the frequency response analysis used to compute the transfer functions. The proportional damping provided damping ratios of approximately 0.5% of critical to all modes in the 0 to 50 Hz frequency range. This provided a small but typical level of damping anticipated in the higher truss modes due to truss joints, boundary conditions and other mechanisms which are difficult to model individually. The damping in the first bending mode pair, shown in Table 6, is significant. It is due to coupling of the actuator modes with the first bending mode pair. Damping in the other truss modes is not affected by the actuators and is due only to proportional damping.

Table 6. Predicted Frequencies and Damping of the Control Configured Truss

Mode	Frequency (Hz)	Damping (%)
Actuators (9)	1.00	10.0
1st X Bending	1.74	1.7
1st Y Bending	1.75	1.7
1st Torsion	6.65	0.5[1]
2nd X Bending	8.45	"
2nd Y Bending	8.45	"
3rd X Bending	19.39	"
3rd Y Bending	19.41	"
2nd Torsion	20.22	"

[1]Proportional damping in model to account for nominal damping in higher modes

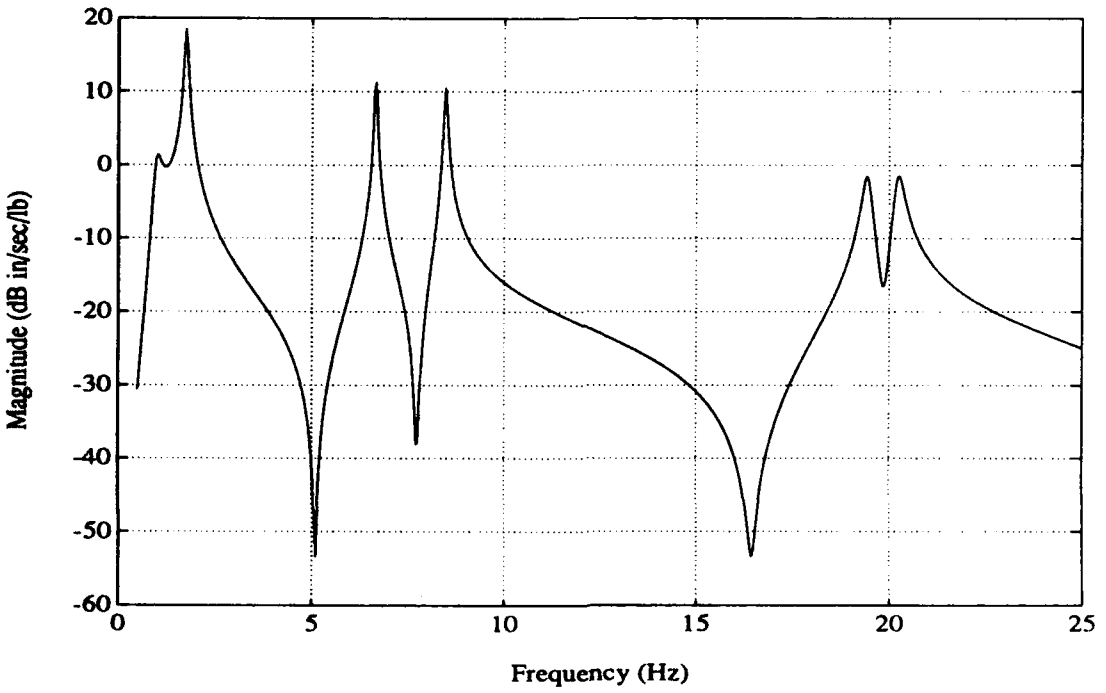

Figure 17. Predicted Transfer Function between Sensor 1 and the Disturbance Actuator

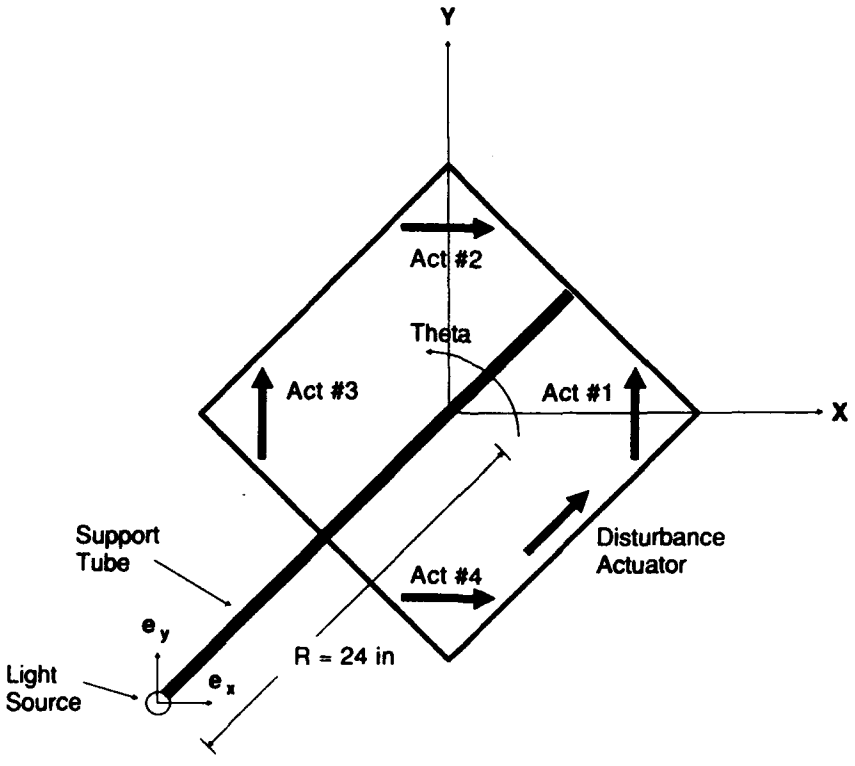

Figure 18. Truss Tip Figure-of-Merit Geometry

4.4 Open-Loop Performance Prediction -- The open-loop response of the truss tip position figure-of-merit was predicted for a random disturbance force at the disturbance actuator. The selection of the performance figure-of-merit for the experiment is discussed in Section 2.5. The X and Y-axis position errors, e_x and e_y, of the truss tip light source in a horizontal plane couldn't be predicted directly since the light source location was not included in the model. Instead, they can be expressed in terms of the X and Y-axis translations, a_x and a_y, and the Z-axis rotation, θ_z, of a point at the center of the truss tip as

$$e_x = a_x + R\,\theta_z \cos 45 \qquad (3)$$

$$e_y = a_y - R\,\theta_z \cos 45 \qquad (4)$$

where R = 24 inches is the distance of the tip light source from the truss axis, assuming small values of θ_z. The truss tip geometry is illustrated in Figure 18.

The rms values of the X and Y-axis position errors, $e_{x_{rms}}$ and $e_{y_{rms}}$, due to a random force input at the disturbance actuator are given by the equations:

$$e_{x_{rms}} = P_{rms} \sqrt{\frac{1}{f_m} \int_0^{f_{max}} |H_x(f)|^2 \, df} \tag{5}$$

$$e_{y_{rms}} = P_{rms} \sqrt{\frac{1}{f_m} \int_0^{f_{max}} |H_y(f)|^2 \, df} \tag{6}$$

where $H_x(f)$ and $H_y(f)$ are the X and Y-axis transfer functions of light source position to disturbance actuator force input and P_{rms} is the rms value of the excitation force in a frequency band with a bandwidth of f_m and a maximum value of f_{max}. The total rms error of the tip light source position, $e_{t_{rms}}$, can then be expressed as:

$$e_{t_{rms}} = \sqrt{e_{x_{rms}}^{\,2} + e_{y_{rms}}^{\,2}} \tag{7}$$

where $e_{x_{rms}}$ and $e_{y_{rms}}$ are defined in equations (5) and (6), respectively.

The disturbance used to predict open-loop performance consisted of a 0 to 50 Hz band random force with an rms amplitude of 1 pound. The disturbance force was applied to the model at the disturbance actuator and transfer functions were computed between the force and truss tip degrees of freedom, a_x, a_y and θ_z. These individual transfer functions were combined using equations (3) and (4) to compute transfer functions $H_x(f)$ and $H_y(f)$, of e_x and e_y to the disturbance input. The X-axis transfer function, $H_x(f)$ is shown in Figure 19. Next, values of $e_{x_{rms}} = e_{x_{rms}} = 0.045$ inch were computed using $H_x(f)$ and $H_y(f)$ in equations (5) and (6). The values are equal because of the near symmetry of the truss configuration. Finally, the total rms error, $e_{t_{rms}} = 0.063$ was computed from equation (7).

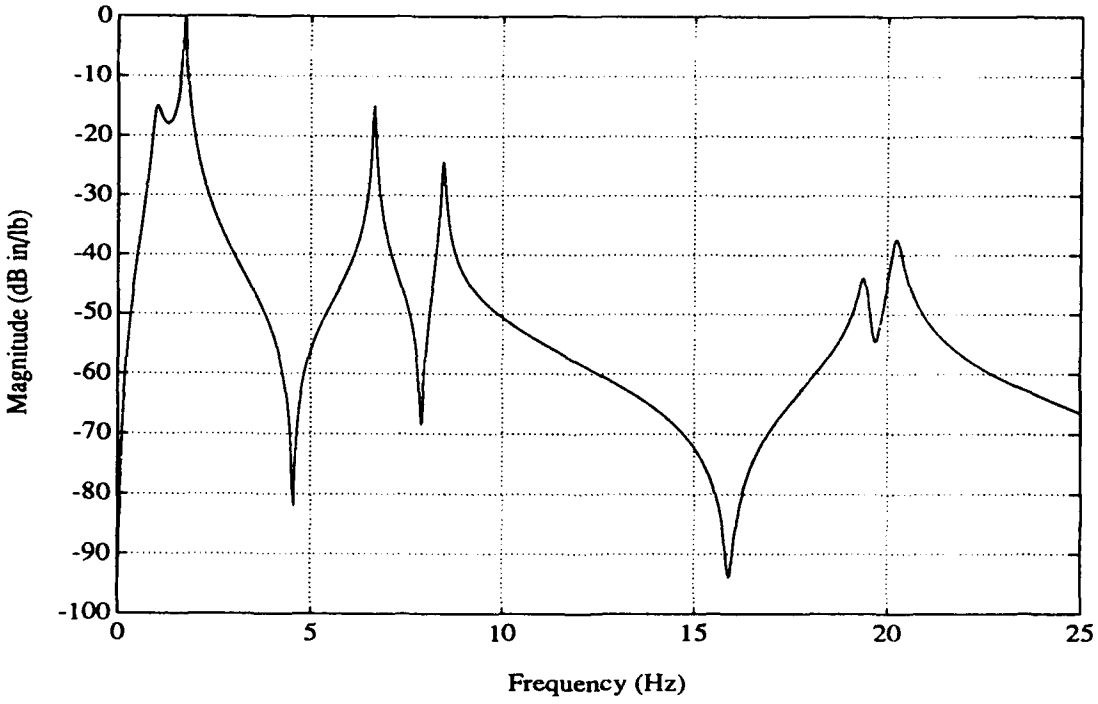

Figure 19. Truss Tip Light Source X-Axis Transfer Function

The total response of the light source figure-of-merit is dominated by the first bending mode pair. This is illustrated by the X-axis transfer function shown in Figure 19. It can be seen from the figure that the first mode peak near 1.75 Hz dominates the response. The Y-axis transfer function is nearly identical because of symmetry. The rms response is computed from equations (5) and (6) as the area under the square of the transfer function, which further increases the relative contribution of the first bending mode. The first bending modes contribute more than 90% of the total truss tip response and should thus receive most of the active control energy.

5.0 DYNAMIC TESTING OF OPEN-LOOP SYSTEM

Extensive dynamic testing was performed on the 12-Meter Truss Active Control Experiment to verify analysis models for active control design and to measure open-loop performance. Natural frequencies, modal damping ratios and transfer functions were identified and open-loop tip figure-of-merit error was measured. This section describes the tests performed and presents the test results.

5.1 Test Procedures -- Several test procedures were used to identify the desired open-loop dynamic characteristics of the experiment. Both stepped sine dwell and continuous random excitation were used to generate transfer functions between selected actuators and sensors. Modal parameters were then identified from the transfer functions. Free decay testing was used to identify frequencies and damping ratios of the actuators and lower order truss modes. The open-loop testing was performed for two values of actuator LVT damping: 10% and 50%. Testing was also done with active feedback cancellation of actuator Coulomb friction. Data acquisition, excitation signal generation and overall test control were performed with the Optima control computer. Data analysis and modal parameter identification were accomplished with Matlab software on the Sun Microsystems workstation.

Averaged transfer functions between the disturbance actuator, and the shaker, and the 8 control sensors were generated for a 0 to 50 Hz band random force input. The force input and sensor output time histories were sampled and stored in the Optima. The disturbance actuator command voltage was also sampled and stored in units of force. This was done because there was no way to directly measure actuator force. For the shaker, input force to the truss was measured by a piezoelectric force gage. Upon completion of the data sampling, the measured time histories were uploaded to the Sun workstation, where transfer functions were computed and plotted. Parameters of modes which appeared to be uncoupled were identified from the transfer functions with the circle fit method [8]. In addition, the time-series method of Hollkamp [9] was used to identify coupled or closely spaced modes and to compare with the circle fit results.

Transfer functions were also generated using a stepped sine dwell method. A sine wave was applied to the disturbance actuator and, after steady state response was achieved, the actuator force command and sensor velocity output signals were sampled. The transfer function magnitude and phase values were computed from the sampled data

using a least squares approach. Then, the excitation frequency was increased by a desired increment and the process was repeated. This test procedure was programmed on the Optima control computer for the desired frequency band and increment. After the test was completed, the computed transfer functions were uploaded to the Sun workstation for parameter identification and plotting.

Free decay response tests were used to identify damping and nonlinearity in the actuator and lower order truss modes. Test conditions consisted of free decay from resonant dwell and from an initial static deflection. The resonant dwell/decay tests were used primarily for the first bending and torsion modes of the truss while the static deflection/decay tests were used for the actuator modes. Again, the Optima was used to generate the disturbance signal, if necessary, and sample and store the data. Frequencies and damping ratios were identified from the decay time records using the method of Agneni and Balis Crema [5].

5.2 Modal Test Results -- Modal testing was performed to generate transfer functions and to identify resonant frequencies and damping ratios of the truss. The testing was done for two levels of LVT feedback actuator damping: 10% and 50%. Stepped sine dwell, band-limited continuous random and free decay test methods were used. These methods were described in Section 5.1.

Transfer functions of velocity/force were measured for inputs to the disturbance actuator, the shaker and actuator 5 (an X-axis actuator at the truss 3/4 station) and outputs from all eight velocity sensors. Both band-limited continuous random and stepped sine inputs were used. Only the random input results are presented here since the random and stepped sine results were very similar.

Results measured for random input to the disturbance actuator and 10% actuator LVT damping will be discussed first. The force input spectrum was gaussian white noise filtered to a 0 to 50 Hz frequency band. The desired rms force level of the input was 1.0 pound, but this value could not be achieved in the test. The actuator drive circuitry was limited to a peak output force of 1.0 pound. A noise input with a gaussian distribution has peak values which can exceed 3 times the rms level, so the maximum achievable rms force was less than 0.33 pounds. A conservative rms force level of 0.2 pound was chosen for the test. The transfer function magnitude for sensor 1 is plotted in Figure 20. The predicted response from the equivalent continuous beam finite element model is also

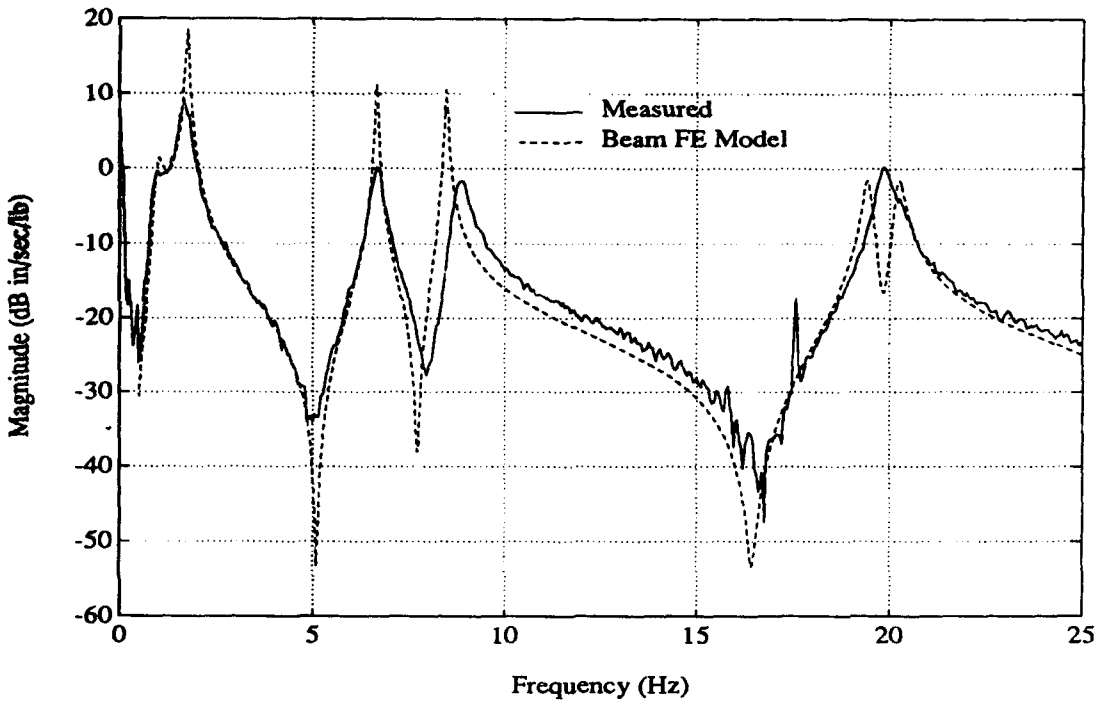

Figure 20. Measured and Predicted Transfer Functions for a Random Input Force to the Disturbance Actuator

shown in the figure. Sensor 1 is a Y-axis sensor at the truss tip (see Figure 3). Three general observations can be made from Figure 20. First, the resonant peaks in the two transfer functions agree fairly well in frequency. This is expected since the finite element model was tuned to match the measured first bending and torsion frequencies of the bare truss. Second, the resonant peak amplitudes of the measured data are significantly lower than the model results. This is probably due, at least in part, to damping mechanisms in the experiment which were not included in the model. Actuator friction is a likely source of unmodelled damping. Characterization of actuator Coulomb friction was discussed in Section 3.4. The third observation from Figure 20 is the high level of noise in the measured data. This is primarily due to the low level of the sampled velocity signal which is a result of the relatively low input force level.

Modal parameters were not identified from the disturbance actuator input test described above, because of the high level of noise present. Instead, a second test was run with a higher input force level to increase the dynamic range and reduce the noise.

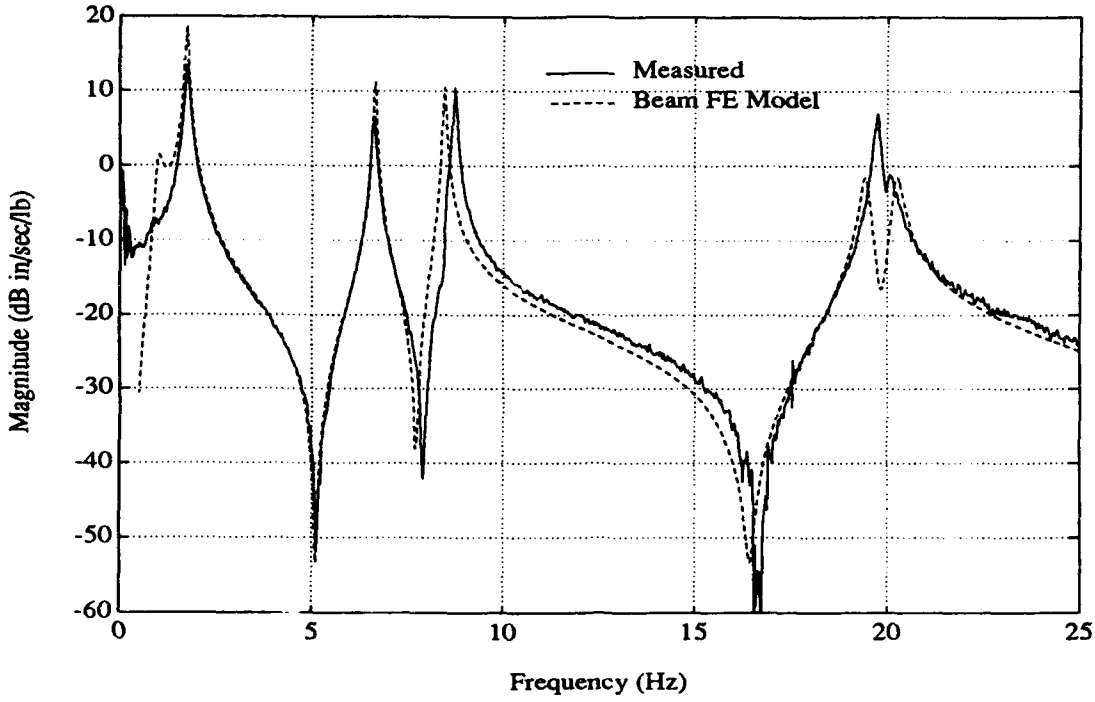

Figure 21. Measured Transfer Function for a Random Force Input to the Disturbance Shaker

An input force of 2.0 pounds rms was achieved by using the disturbance shaker at the truss tip. The transfer function magnitude for sensor 1 and shaker force input is plotted in Figure 21 with the predicted results from the model. As expected, the measured data in the figure are noticeably less noisy than the disturbance actuator input data shown in Figure 20. It should be noted that results from the shaker and disturbance actuator input cases are not directly comparable. A force command to the shaker produces only the desired input force. But, a force command to the disturbance actuator produces the desired force on the structure as well as an equal and opposite force on the actuator moving mass. The force on the moving mass is coupled to the truss dynamics by the actuator centering springs and LVT feedback damper. This coupling only affects the low frequency modes of the system, i.e., the first truss bending pair and the actuator modes. The coupling effect can be seen in the disturbance actuator data of Figure 20 as the small peak near 1.0 Hz. This peak is not present in the shaker data for the model shown in Figure 21.

The measured transfer function shown in Figure 21 agrees well with the model

results in the 0 to 10 Hz control bandwidth. The first Y-axis bending mode peak at 1.75 Hz and the first torsion model peak at 6.65 Hz match up very well with the model. Again, the agreement should be good since the model was tuned to test data. The peak amplitude agreement with the model is improved over the disturbance actuator input case. All the resonant peaks in the shaker input transfer function have significantly higher amplitude than the disturbance actuator input data. This appears to be an amplitude dependent nonlinearity in the system caused by Coulomb friction in the actuators. The two modes near 20 Hz, third Y-axis bending and second torsion, do not agree with the model. This is not important for active control design, however, since these modes have virtually no effect on the control figure-of-merit.

Frequencies and modal damping ratios were identified from the shaker input transfer functions using the circle fit method [8]. The resulting values are listed in Table 7 along with values identified from the model, which were previously listed in Table 6. Also shown in the table are values identified using the time-series method of Hollkamp [9]. The frequencies from the measured data are very close to the model frequencies. The damping ratios also agree very well, except for the first bending mode pair. For these two modes, the measured damping ratios are approximately twice the predicted values. This can be attributed to unmodelled sources of damping in the structure, including Coulomb friction in the actuators. The Coulomb friction damping in the actuators is amplitude dependent. The effective damping in the actuators at the relatively low amplitudes of the random force input tests would be much higher than the damping measured during actuator characterization, which was done at high actuator moving mass amplitudes. The frequency and damping ratio for a single actuator mode, identified with the time-series method, are shown in the table. The nine actuator modes are nearly coincident in frequency and are, therefore, practically impossible to identify from single input excitation. Identification of these modes was accomplished using a free decay test on each actuator.

Frequencies and damping ratios were identified from free decay time histories of truss response to compare with the frequency domain estimates. The results of the free decay tests are listed in Table 7 with the frequency domain, circle fit and time-series model results. The table shows good agreement between the two identification methods for both frequencies and damping ratios. A typical decay response time history is shown in Figure 22. The figure shows velocity response from sensor 1 for the first Y bending mode. The free decay results were also used to investigate the linearity of the structural

Table 7. Predicted and Measured Frequencies and Damping of the Control Configured Truss

Mode	Beam Model		Circle Fit		Free Decay		Time-Series	
	f_d (Hz)	ζ (%)	f_d (Hz)	ζ (%)	f_d (Hz)	ζ (%)	f_d (Hz)	ζ (%)
Actuators (9)	1.00	10.0	-	-	0.91[1]	10.4 - 24.2[1]	0.92[2]	5.0[2]
1st X Bending	1.74	1.7	1.75	3.8	1.72	3.7	1.65	2.4
1st Y Bending	1.75	1.7	1.77	3.3	1.75	3.8	1.73	3.7
1st Torsion	6.65	0.5[3]	6.61	0.5	6.63	0.6	6.57	1.3
2nd X Bending	8.45	"	8.48	0.5	8.51	0.6	8.49	0.8
2nd Y Bending	8.45	"	8.74	0.7	8.76	0.6	8.67	1.1
3rd X Bending	19.39	"	19.20	0.4	19.23	0.5	19.21	0.5
3rd Y Bending	19.41	"	19.72	0.2	19.77	0.4	19.69	0.8
2nd Torsion	20.22	"	20.06	0.2	20.12	0.5	19.98	0.8

[1]Range of values from tests of each actuator on the truss

[2]Only one mode can be identified from single input data

[3]Proportional damping in model to account for nominal damping in the truss higher modes

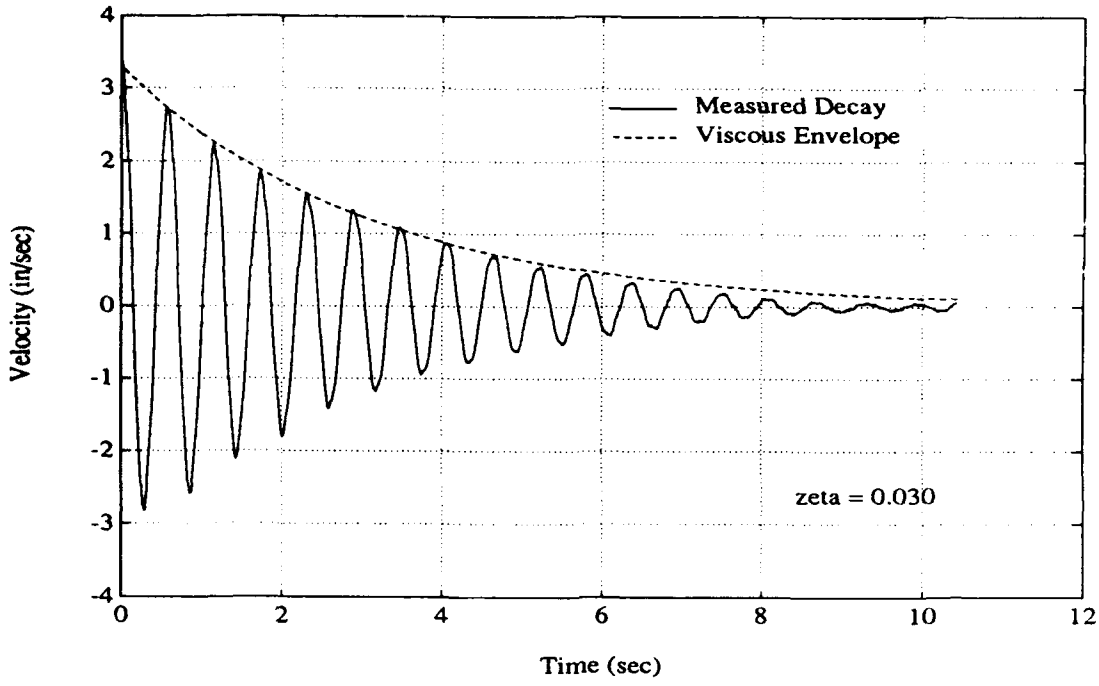

Figure 22. Free Decay Time History of 1st Y-Axis Bending Mode -- 1.75 Hz

response with amplitude. An indication of amplitude nonlinearity was shown in the transfer functions as previously discussed. The decay envelope for a linear, viscous damped mode is plotted in Figure 22 for comparison. The measured data in the figure follow the viscous envelope reasonably well. There is, however, some indication of an amplitude nonlinearity. The nonlinearity is most likely Coulomb friction damping since there is significant actuator moving mass displacement (relative to its base) in the mode shapes of the first pair of bending modes.

The open-loop modal characteristics of the experiment were also identified for the case of 50% actuator damping. Band limited random input to the disturbance shaker was used with frequency domain, circle fit identification. The magnitude of a typical transfer function from sensor 1 is shown in Figure 23. The 10% damping case is also plotted in the figure for comparison. The only significant difference in the two curves shown in the figure is the lower amplitude of the resonant peaks of the 50% damping case in the 0 to 10 Hz bandwidth. The reduced resonant amplitude should be due to the increased actuator damping effect on the low frequency structural modes. Frequencies and modal damping ratios were identified from the 50% damping data and are listed in

Table 8. Measured Frequencies and Damping of the Truss with 10% and 50% Actuator Damping

Mode	10% Actuator Damping		50% Actuator Damping	
	f_d (Hz)	ζ (%)	f_d (Hz)	ζ (%)
1st X Bending	1.75	3.8	1.73	8.4
1st Y Bending	1.77	3.3	1.75	5.6
1st Torsion	6.61	0.5	6.60	0.8
2nd X Bending	8.48	0.5	8.50	0.6
2nd Y Bending	8.74	0.7	8.75	0.7
3rd X Bending	19.20	0.4	19.23	0.5
3rd Y Bending	19.72	0.2	19.75	0.4
2nd Torsion	20.06	0.2	20.11	0.8

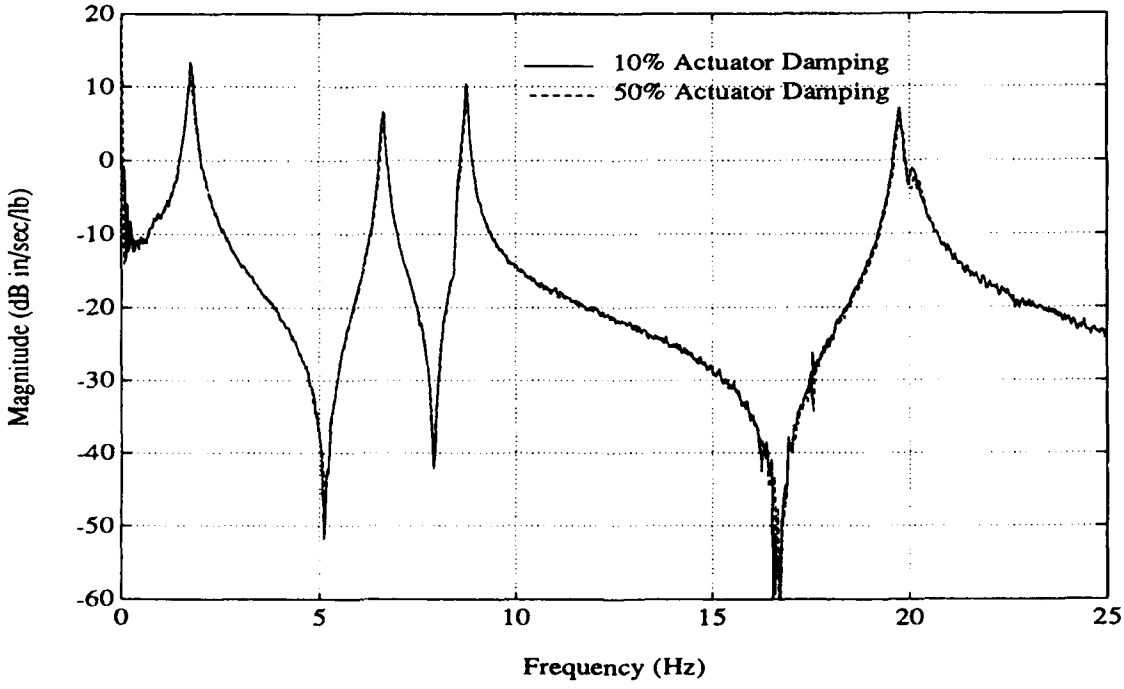

Figure 23. Measured Transfer Function for a Randon Force Input to the Disturbance Shaker -- 10% and 50% Actuator Damping

Table 8 with the results from the 10% case for comparison. No actuator modes were identified from the 50% damping random input case.

5.3 Active Friction Cancellation Results -- An effort was made to actively cancel the Coulomb friction forces in the actuators because the friction added considerable unmodelled damping to the first truss bending mode pair. First, each actuator was tested to identify the Coulomb friction force and viscous damping ratio. Then, the friction force was cancelled by feeding back the moving mass relative velocity signal though the Optima control computer with a simple algorithm. This section describes the friction cancellation scheme and the resulting truss modal parameters.

Identification of the Coulomb friction forces and viscous damping ratios of the eight control actuators was discussed in Section 3.4. The identified parameters are listed in Table 2. The active friction cancellation was implemented in the Optima by sensing the moving mass relative velocity (from the LVT) and commanding a constant force to the actuator equal to 90% of the measured friction force and with the same algebraic sign as the relative velocity. The value of 90% was chosen to be conservative. This left 10% of the original friction force as a margin in case the identification was slightly in error and would help prevent a potential instability due to a net negative friction force.

The measured Coulomb friction forces and viscous damping ratios for actuators 1 and 2 with active friction cancellation are shown in Table 9. The values for the actuators without friction cancellation are shown in the table for comparison. Also shown in the table are the effective viscous damping ratios of the actuators with and without friction cancellation. The friction force value of 0.002 pound for actuator 1 with active cancellation is roughly 10% of the nominal value of 0.017 pound, just as it was designed to be. The effective viscous damping ratio of the actuator decreased from 0.104 to 0.043 due to the reduced friction force and its contribution to effective viscous damping. This is illustrated in Figure 24 where an actuator free decay response with friction cancellation is plotted with the response of a purely viscous model. The agreement is very good. The values in Table 9 for actuator 2 follow the same trends as actuator 1. The friction cancellation effects on the actuator do pose some questions, however. The viscous damping coefficient of actuator 1 increased with friction cancellation from 0.046 to 0.055 pound/inch/second. This increase cannot be explained. Furthermore, the viscous damping ratio with active friction cancellation of 0.055 is larger than the total effective viscous damping ratio of 0.043 which should also include some friction effect. This is

Table 9. Actuator Viscous Damping Ratios and Coulomb Friction Forces with Active Friction Cancellation

		Nominal Actuator			Active Friction Cancellation		
Actuator	f_d	ζ^1	F_c (lb)[2]	ζ_{eff}^3	ζ^1	F_c (lb)[2]	ζ_{eff}^3
1	0.91	0.046	0.017	0.104	0.055	0.002	0.043
2	"	0.024	0.041	0.242	0.053	0.004	0.064

[1] Measured by the resonant dwell method

[2] Coulomb friction force measured by resonant dwell method

[3] Effective viscous damping ratio measured from free decay data

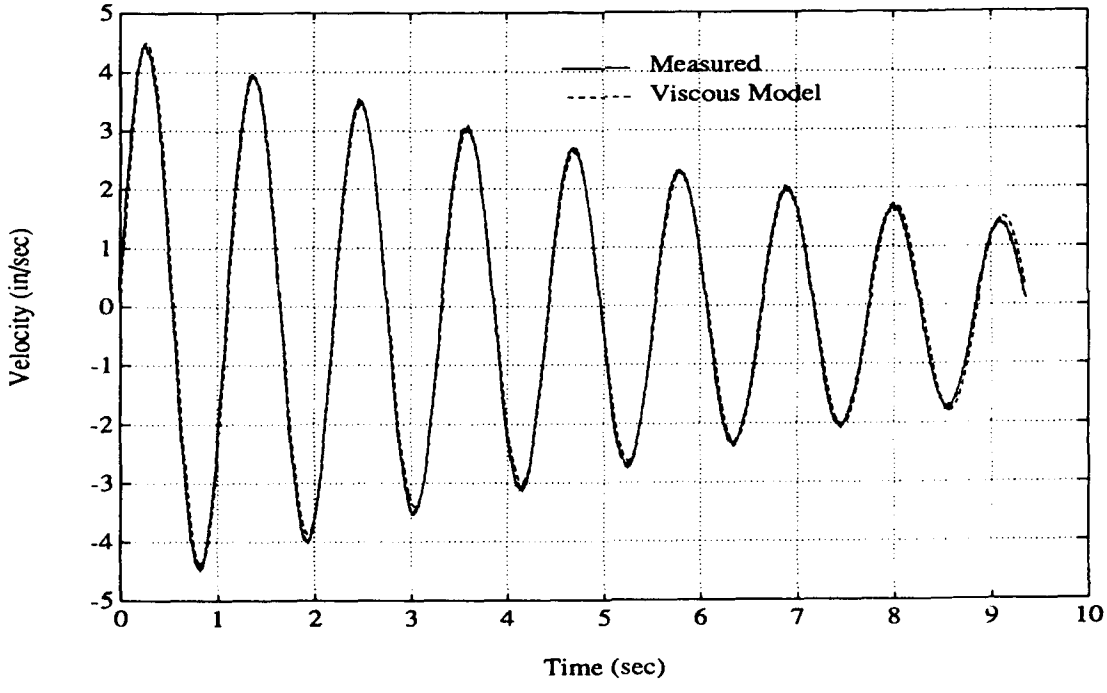

Figure 24. Free Decay Response of Actuator 1 with Active Friction Cancellation

clearly unexpected but can be attributed to damping mechanisms in the actuator in addition to Coulomb friction and viscous damping. In any case, the actuator response with active friction cancellation can be considered viscously damped. It would be simple, then, to add viscous damping via LVT feedback to achieve any desired value of viscous damping in the actuator mode.

Resonant frequencies and modal damping ratios of the truss modes with active friction cancellation in the actuators were identified from transfer functions generated with random noise input to the disturbance shaker. The results of this test are shown in Table 10. The damping ratios for the first bending mode pair are considerably lower than the values from the truss without friction cancellation also shown in the table. The effect of active friction cancellation is also evident in the free decay response of the first bending mode, shown in Figure 25 with a purely viscous decay model response. The effect of friction cancellation is evident as a lower damping ratio, as shown in the figure, but the measured decay trace does not agree with the viscous model any better than the truss without friction cancellation previously shown in Figure 22. Some low frequency modulation of the measured decay data is present in the figure. This modulation makes it difficult to judge the degree of agreement with the model. An attempt was made to directly identify the Coulomb friction force affecting the first Y bending mode using the SDOF method described in Section 3.4. The results of this test were inclusive, however.

5.4 Performance Test Results -- The rms position error of the truss tip figure-of-merit was measured in the presence of a 0 to 50 Hz band random noise input to the disturbance shaker. The input spectrum had an rms level of 1 pound force. The position error was measured by the optical sensor at the truss base. The performance figure-of-merit and optical sensor are described in Sections 2.5 and 3.5, respectively.

The measured rms response of the truss tip figure-of-merit in the 10% actuator damping configuration is 0.028 inch. The value predicted from the equivalent beam finite element model is 0.063 inch, which is considerably higher than the measured value. The low measured response is probably due to two factors; higher than predicted damping in the first truss bending mode pair and low shaker force input at the first bending mode frequency. The first pair of bending modes at 1.75 Hz contributes more than 90% of the response to the truss tip figure-of-merit response as was discussed in Section 4.4. The modal damping ratios measured for these modes were 0.038 and 0.033 which is much higher than the 0.017 value predicted from the model. It is clear, then,

Table 10. Measured Frequencies and Damping of the Truss with Active Friction Cancellation

Mode	10% Actuator Damping f_d (Hz)	ζ (%)	Active Friction Cancellation f_d (Hz)	ζ (%)
1st X Bending	1.75	3.8	1.78	2.6
1st Y Bending	1.77	3.3	1.77	2.1
1st Torsion	6.65	0.5	6.64	0.6
2nd X Bending	8.48	0.5	8.50	0.4
2nd Y Bending	8.74	0.7	8.76	0.3
3rd X Bending	19.20	0.4	19.25	0.4
3rd Y Bending	19.72	0.2	19.81	0.4
2nd Torsion	20.06	0.2	20.21	0.4

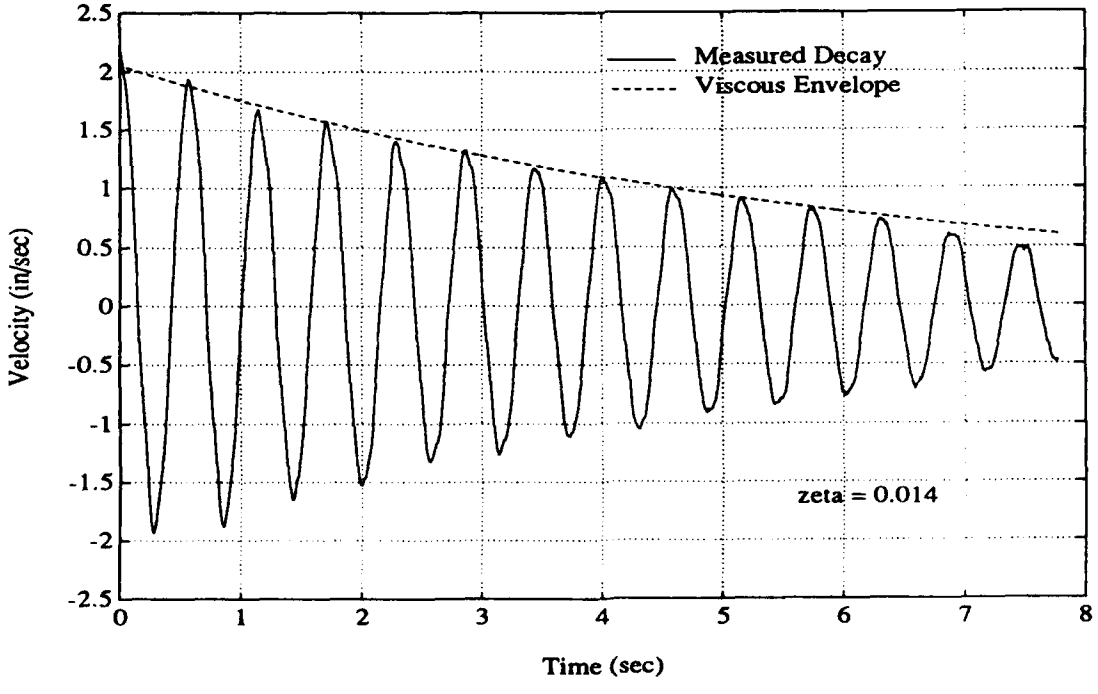

Figure 25. Free Decay Time History of 1st X-Axis Bending Mode with Active Friction Cancellation

that the measured tip response should be lower due to the higher damping present in the truss. The effect of damping in the first bending modes on truss tip response can be seen by looking at the figure-of-merit response level for the truss with active friction cancellation. The measured rms tip response with friction cancellation is 0.038 inch while the damping ratios for the first bending modes are 0.026 and 0.021. However, these damping ratios are still higher than the 0.017 predicted from the model. The second factor contributing to a lower than predicted open-loop tip response is reduced disturbance shaker force at low frequency. The desired input force spectrum is a constant level in a 0 to 50 Hz frequency band with an rms value of 1.0 pound. The measured force spectrum from the shaker rolled off significantly below 5 Hz. The force spectrum level at the 1.75 Hz first bending mode pair is approximately 60% of the desired spectrum level. The roll-off of shaker force at frequencies below 5 Hz is due to the dynamics of the electromagnetic shaker itself. The effect of reduced shaker force can be illustrated by computing the rms response of the tip figure-of-merit with the input force reduced by 33% below 5 Hz. The predicted value is 0.043 inch rms. This value agrees better with the 0.038 inch measured with active friction cancellation. A potential solution to the low force problem would be to filter the force command to the shaker with a spectral window shaped to amplify the low frequency region.

In summary, the measured rms response of the truss tip figure-of-merit is lower than the value predicted by the model. This difference can be adequately explained by the higher than predicted damping in the first bending mode pair and the lower than desired input force at the first bending mode pair frequency. The measured open-loop tip response was used later to compare with the closed-loop response of several active controllers to judge controller effectiveness. The 0.038 inch rms value from the active friction cancellation case was selected as the open-loop baseline because this case has lower first mode pair damping values which are more representative of the low modal damping values anticipated in future space structures.

6.0 CONCLUSIONS

This report has presented the results of the design, hardware configuration, analysis and open-loop testing of the 12-Meter Truss Active Control Experiment. Design and testing of closed-loop controllers are described in [1]. The experiment development activity resulted in a well characterized, representative test bed for the evaluation of active vibration control and identification approaches for future large space structures. Several specific conclusions have been reached on the various aspects of the experiment. These conclusions will be discussed in detail in the following paragraphs.

6.1 Experiment Design and Hardware -- The 12-Meter Truss Active Control Experiment met most of the design goals described in Section 2.1. The 1.75 Hz first bending mode frequency was close to the 1 Hz design goal and the truss had five flexible modes below 10 Hz which provided a reasonable modal density at low frequencies. The goal of modal damping ratios less than 1% of critical was met by the bare 12-meter truss, but damping ratios in the truss with actuators were somewhat higher than desired. The performance figure-of-merit selected for the experiment, i.e., displacement in a horizontal plane of a point light source offset to the side of the truss tip, was effective as a control design objective and proved easy to measure for closed-loop performance testing. However, the fact that the figure-of-merit response was dominated by the single pair of first bending modes made the experiment somewhat less interesting than it could have been. Having a significant contribution to the figure-of-merit response from several dissimilar modes would make the control design process more challenging. It might also give the midstation control actuators more authority. Since only the first bending modes needed to be controlled, the tip actuators did the majority of the work while the four midstation actuators were not as effective. The last design goal, that of an unconstrained structure, was not achieved in the experiment due to practical considerations. The frequencies of the unconstrained 12-meter truss were too high to meet the frequency goal and adding mass to lower the frequencies was not practical. Use of another truss structure was not considered because of the expense of design and fabrication. The desire for an unconstrained structure was not critical to the experiment for demonstration of active control approaches.

The sensors and actuators selected for the experiment performed well during open-loop testing. The velocity sensing approach, implemented with piezoelectric accelerometers and analog integration circuitry, provided reasonable signals for

identification and control purposes. The sensors had good low frequency response and an acceptable noise level. More gain and lower noise from the sensors are desirable, though. The fixed input range of the Optima control computer coupled with the relatively low gain of the integrator circuitry resulted in a less than desirable signal-to-noise ratio in the velocity signals The accelerometer/integrator combination also produced a drift in the sensor signals at very low frequencies which was passed through the control computer to the actuators in closed-loop control. Replacement of the accelerometers with high sensitivity, low noise units like the Sunstrand QA-1400 is recommended to improve both the signal-to-noise and low frequency drift problems.

The linear momentum exchange actuators and relative velocity feedback damping circuitry performed very well. They had good low frequency response and were well suited to use on an active control testbed. Friction in the actuator linear bearings was the source of nonlinear damping in the actuators which affected the lowest frequency truss bending modes. The added damping should have a negligible effect on active controller performance, though. A simple, effective approach was developed to simultaneously identify the Coulomb friction force and the viscous damping coefficient of each actuator. In addition, an active friction cancellation scheme was demonstrated which effectively eliminated the friction damping. Even though the actuators performed very well in the experiment, these devices are not well suited for use in real structures at frequencies below 10 Hz. Their low ratio of force output to total mass and the travel required for moving mass motion make them impractical for operational systems.

The number and location of collocated sensor and actuator pairs on the truss was adequate to provide effective control of the truss tip position figure-of-merit. The locations were chosen to provide sensing and actuation for the first few truss bending and torsion modes. A formal actuator placement scheme was not used but may be useful in the future if a performance or weight optimal experiment design is needed.

The approach for measuring the truss tip position error figure-of-merit performed very well. The combination of an offset tip light source imaged by a two-dimensional optical sensor at the truss base gave an accurate and repeatable measurement of truss motion. It was important that the control performance objective be measurable for experimental verification of active controller performance. The optical sensor arrangement was simple and inexpensive and yet was capable of resolving light source motion to less than 0.001 inch at a distance of 40 feet.

The Optima real-time control computer was very effective in the open-loop characterization of the experiment. The Optima system was used to generate disturbance signals, acquire and store truss response data, perform limited near real-time data analysis, and conduct off-line parameter identification. The Optima was also used to implement the nonlinear active friction cancellation algorithm described in Section 5.3. The C language programming capabilities of the Optima allow the implementation of a wide range of real-time and near real-time control and identification algorithms. One weakness of the Optima for sampled data parameter identification applications is the lack of antialiasing filters on the inputs channels. This was not a problem in open-loop testing of the truss. Frequency content of the sensor signals above the 50 Hz Nyquist frequency was low enough that aliasing was not a problem.

6.2 Dynamic Analysis -- Open-loop dynamic analysis of the experiment was performed with an equivalent continuous beam finite element model as described in Section 4.2. The beam model was composed of 16 beam elements, one for each truss bay. Actuators were modelled as SDOF systems coupled to the beam model. The beam model was reasonably accurate compared to a full frame model of the truss and allowed normal mode analysis on a personal computer in a few minutes and frequency response calculation in less than an hour. Fundamental bending and torsion frequencies of the beam model were independently tuned to match measured values from the bare truss. No attempt was made to tune the model with measured mode shape information. The beam model was used to compute normal mode frequencies and mode shapes, frequency domain transfer functions, and rms tip position figure-of-merit error.

6.3 Open-Loop Testing -- Open-loop testing was conducted on the experiment to identify modal parameters and to measure tip position figure-of-merit error in the presence of a random disturbance input. Tests were conducted on the truss with 10% and 50% actuator damping and with active friction cancellation in the actuators. Modal parameters were identified from time domain and frequency domain response data.

In general, measured frequencies agreed very well with predictions from the equivalent beam finite element model. Frequency agreement was best for the lowest frequency modes. This was expected since the model was tuned to match the first bending and torsion frequencies of the bare truss. The agreement of higher modes was not as good, but was adequate for preliminary control design purposes. Measured modal

damping ratios did not agree well with predictions for the first pair of truss bending modes. The poor agreement can be attributed to unmodelled damping in the truss, primarily Coulomb friction from the actuator moving mass linear bearings. Other unmodelled sources of damping were not identified but were surely present. These other sources could include instrumentation wiring, base mounting interface effects and disturbance shaker bearing friction.

An effective method of actively cancelling most of the actuator Coulomb friction was demonstrated. The approach combined a simple method to identify the friction force in each actuator with a direct force cancellation algorithm implemented in the Optima control computer. The active friction cancellation approach reduced the measured modal damping in the first bending mode pair from over 3% of critical to near 2%. Modal damping in a future large space structure will be valuable whether it comes passively from an actuator or actively as part of a control law. An important requirement is that the damping mechanism be included in the control design model. Therefore, elimination of friction is important to eliminate its nonlinear effects which cannot be adequately included in a linear model.

REFERENCES

1. Ozguner, U., Yurkovich, S., et. al.,"Vibration Control Experiments on a 12-Meter Cantilever Truss Structure," Air Force Wright Laboratory Technical Report WL-TR-92-3024, April 1992.

2. Ozguner, U., Yurkovich, S. and Gordon, R., "A Case Study in Control Design and Implementation for Flexible Structure Systems," 1989 American Control Conference, Pittsburg, PA, June 1989.

3. Gehling, R., Morganthaler, D. and Richards, K., "Passive and Active Control of Space Structures (PACOSS)," Air Force Wright Laboratory Technical Report WL-TR-91-3052, June 1991.

4. Wright, N., Barker, S., Taylor, K. and Tung, F., "Vibration Control of Space Structures (VCOSS II)," Air Force Wright Aeronautical Laboratories Technical Report AFWAL-TR-86-3073, September 1986.

5. Agneni, A. and Balis Crema, L., "Analytic Signals in the Damping Coefficient Identification," Proceedings of the European Space Agency Conference on Spacecraft Structures and Mechanical Testing, Noordwijk, The Netherlands, October 1988, pp. 133-139.

6. Tse, F., Morse, I. and Hinkle, R., *Mechanical Vibrations*, Allyn and Bacon, Inc., Boston, 1963, pp. 175-178.

7. Gordon, R., "Identifying Viscous Damping and Coulomb Friction in the 12-Meter Truss Actuator," Air Force Wright Laboratory Technical Memorandum WL-TM-91-325-FIBG, July 1991.

8. Ewins, D. and Vakakis, A., "An Alternate Method for SDOF Modal Analysis," The International Journal of Analytical and Experimental Modal Analysis, Volume 4, Number 4, pp. 144-149, October 1989.

9. Hollkamp, J., "Multiple-Input Multiple-Output Time-Series Models from Short Data Records," Paper No. 91-0994, Proceedings of the AIAA 32nd Structures, Structural Dynamics and Materials Conference, Baltimore, MD, April 1991.

U.S. Government Printing Office 648-127